Retinoic acid temporally orchestrates colonization of the gut by vagal neural crest cells

Rosa A. Uribe, Stephanie S. Hong, Marianne E. Bronner

www.elsevier.com/locate/developmentalbiology

PII: S0012-1606(17)30719-4
DOI: https://doi.org/10.1016/j.ydbio.2017.10.021
Reference: YDBIO7618

To appear in: *Developmental Biology*

Received date: 10 October 2017
Accepted date: 23 October 2017

Cite this article as: Rosa A. Uribe, Stephanie S. Hong and Marianne E. Bronner, Retinoic acid temporally orchestrates colonization of the gut by vagal neural crest cells, *Developmental Biology,* https://doi.org/10.1016/j.ydbio.2017.10.021

Retinoic acid temporally orchestrates colonization of the gut by vagal neural crest cells

Rosa A. Uribe[a,b1*], Stephanie S. Hong[a1], Marianne E. Bronner[a]

[a]Division of Biology and Biological Engineering, California Institute of Technology, Pasadena, California 91125, USA

[b]Department of Biosciences, Rice University, Houston TX 77005, USA

[*]Correspondence should be addressed to R.A.U., rosa.uribe@rice.edu

Running head: Retinoic acid temporally regulates ENS formation

Key words:

Retinoic Acid, neural crest, meis3, zebrafish, enteric nervous system

Summary

The enteric nervous system arises from neural crest cells that migrate as chains into and along the primitive gut, subsequently differentiating into enteric neurons and glia. Little is known about the mechanisms governing neural crest migration en route to and along the gut *in vivo*. Here, we report that Retinoic Acid (RA) temporally controls zebrafish enteric neural crest cell chain migration. *In vivo* imaging reveals that RA loss severely

[1] These authors contributed equally

compromises the integrity and migration of the chain of neural crest cells during the window of time window when they are moving along the foregut. After loss of RA, enteric progenitors accumulate in the foregut and differentiate into enteric neurons, but subsequently undergo apoptosis resulting in a striking neuronal deficit. Moreover, ectopic expression of the transcription factor *meis3* and/or the receptor *ret*, partially rescues enteric neuron colonization after RA attenuation. Collectively, our findings suggest that retinoic acid plays a critical temporal role in promoting enteric neural crest chain migration and neuronal survival upstream of Meis3 and RET *in vivo.*

Impact statement: A novel stage-specific role for Retinoic Acid in enteric neural crest migration and neuronal survival along the developing gut *in vivo*

Introduction

The enteric nervous system (ENS) is a network of thousands of interconnected ganglia, located within the myenteric and submucosal plexuses of the gut wall, that regulates peristalsis, secretions and water balance (Furness, 2006; Bergeron et al., 2013). As the largest division of the peripheral nervous system, the mature ENS contains hundreds of millions of neurons, surpassing the number found in the spinal cord

(Furness, 2006). In particular, the ENS is the only major population of neurons outside of the central nervous system with circuits that perform autonomous reflex activity. In humans, defects in ENS formation lead to pediatric disorders such as *Hirschsprung Disease (*HSCR*)*, also known as gut aganglionosis, which is characterized by a paucity of ganglia along variable lengths of the gut. Colonic aganglionosis is the most common form of HSCR, occurring every 1 in 5000 births (Obermayr et al., 2012; Bergeron et al., 2013). The current treatment is surgical resection of the aganglionic intestinal segment (Bergeron et al., 2013); however eventual outcomes of patients varies greatly and most exhibit functional enteric defects throughout life—highlighting the need for alternative treatments and understanding the ontogeny of both normal and abnormal ENS development.

During development, the ENS is largely derived from “vagal” neural crest cells that arise dorsally in the post-otic neural tube at early stages of central nervous system formation (Le Douarin et al., 1973; Epstein et al., 1994; Kuo and Erickson, 2011). Neural crest cells are a group of multipotent stem cells that undergo an epithelial to mesenchymal transition (EMT) and embark on migratory routes in order to reach their final and often distant destinations throughout the embryonic body (Saint-Jeannet, 2006; Green et al., 2015). During development, neural crest cells give rise to various types of specialized tissues, including craniofacial cartilage, peripheral neurons and glia, pigment cells and dental tissues (Green et al., 2015). During their initial journey, vagal neural crest emigrate from the neural tube at axial levels adjacent to somites 1-7, migrate ventrally and, after entering the foregut mesenchyme, migrate in chains along its rostrocaudal extent until they reach the hindgut (Le Douarin and Teillet, 1973; Peters-Van Der Sanden et al., 1993; Burns et al., 2000; Tucker et al., 1986; Anderson et al., 2006).

The process of gut invasion by vagal neural crest is largely conserved across jawed vertebrates, though the ENS is simpler in zebrafish than in amniotes (Shepherd et al., 2004; Heanue et al., 2016; Ganz et al., 2016). By 32 hours post fertilization (hpf), zebrafish vagal neural crest cells commence migration medially toward the foregut as two chains and migrate caudally along the left and right sides of the gut tube to fully colonize the hindgut by 72 hpf (Kelsh and Eisen, 2000; Dutton et al., 2001; Shepherd et al., 2001; Elworthy et al., 2005; Olden et al., 2008; Uribe and Bronner, 2015). Within the gut environment, neural crest cells are referred to as 'enteric neural crest'. To ensure proper numbers of enteric progenitors, enteric neural crest proliferate extensively and undergo terminal differentiation to give rise to glia and numerous classes of enteric neurons—such as motor, sensory and interneurons (Furness, 2006; Sasselli et al., 2012). Ultimately, enteric neurons terminally differentiate into subtypes, such as serotonergic (5HT), catecholaminergic and Nitric Oxide (NO)-containing neurons (Sasselli et al., 2012; Uesaka et al., 2016).

Mutations have been identified in several genes that contribute to HSCR and are required for ENS development (Zimmer and Puri, 2015; Bergeron et al., 2013). These include the receptor tyrosine kinase *Ret,* expressed on vagal neural crest cells, and its ligand, *Glial Cell-line Derived Neurotrophic Factor* (GDNF). *Ret* mutations cause total intestinal aganglionosis and are known to be the most common cause of HSCR in humans; the conservation of this function has been demonstrated in numerous model organisms, such as mouse and zebrafish (Natarajan et al., 2002; Pachnis et al., 1998; Jain et al., 2004; Heanue et al., 2008). Similar to *Ret*$^{-/-}$*, GDNF*$^{-/-}$ mice lack almost all enteric ganglia (Taraviras and Pachnis, 1999; Sanchez et al., 1996; Moore et al., 1996; Pichel et al., 1996). Additionally, loss of genes that encode conserved transcription

factors *Sip1*, *Sox10*, *Foxd3*, *Tfap2α* and *Pax3* cause reduction or loss of vagal neural crest cells, along with defects in the ENS and other parts of the peripheral nervous system (Southard-Smith et al., 1998; Kapur, 1999; Lang et al., 2000; Wakamatsu et al., 2001; Knight et al., 2003; Montero-Balaguer et al., 2006; Carney et al., 2006).

While these studies identify some transcription factors and receptors/ligands critical for ENS development, events that control the timing of enteric neural crest migration and differentiation along the gut are less well understood. Outstanding questions remain regarding the temporal signals and their downstream mediators that regulate enteric neural crest migration en route to and along the gut. These events are difficult to investigate in amniotes since the gut is semi-opaque and problematic to visualize. While studies of gut explants have made it possible to analyze the speed, directionality and frontal expansion of the enteric neural crest during both their individual and collective cell migration (Druckenbrod and Epstein, 2005; Young et al., 2014), far less is known about the molecular or temporal mechanisms underlying this migration.

One signal that has been suggested to influence enteric neural crest development is Retinoic Acid (RA). For example, in mouse embryos, knockout of retinaldehyde dehydrogenase *Aldh1a2* (formerly *Raldh2*), the enzyme responsible for generation of RA, results in complete failure of ENS formation due to the catastrophic loss of vagal neural crest cells (Niederreither et al., 2003). Consistent with this, studies in cell and explant cultures have shown that RA treatment affects enteric neural crest migration (Simkin et al., 2013; Fu et al., 2010), proliferation and/or neuronal differentiation (Sato and Heuckeroth, 2008). However, it remains unclear when RA is affecting enteric neural crest migration or what downstream transcriptional effectors are involved. These

events are particularly difficult to study in amniotes due to the inaccessibility of intact gut tissue to live imaging.

To address these questions *in vivo*, we have turned to zebrafish embryos due to their ease of manipulation and optical clarity that enables visualization of the process of enteric neural crest migration in real time. Utilizing pharmacological and genetic modulation of the RA pathway, combined with live imaging and epistasis experiments, we examine the temporal role of the RA pathway during early ENS development. The results reveal a novel mechanism whereby RA functions to temporally influence migration of enteric neural crest and neuronal survival upstream of the transcription factor Meis3 and the RET receptor *in vivo*.

Results

RA pathway components are expressed in the gut during enteric neural crest migration

As a first step in investigating the role of RA signaling in zebrafish enteric nervous system development *in vivo*, we examined the distribution of RA pathway components involved in RA synthesis and turnover along the gut during enteric neural crest migration. To this end, we performed *in situ* hybridization to examine the spatial distribution of the following transcripts at 48 hpf: *aldehyde dehydrogenase 1 family, member A2 (aldh1a2), retinol binding protein 1a, cellular (rbp5)* and *cellular retinoic acid binding protein 2, a (crabp2a)*. While retinol-binding proteins are involved in the transfer of retinol, the RA precursor also known as Vitamin A, aldehyde dehydrogenase enzymes are responsible for the synthesis of RA from retinol and Crabp proteins balance the intracellular levels of RA to mediate feedback and degradation of RA (Schilling et al.,

2012; Barber et al., 2014). In particular, we focused on their expression along the foregut, midgut and hindgut, as depicted schematically in **Figure 1A**.

aldh1a2 was detected at all levels of the gut at 48 hpf (**Fig. 1B;** arrows). Similarly, *rbp5* was observed along the entire gut at 48 hpf (**Fig. 1C**), while *crabp2a* was primarily localized to the foregut (**Fig. 1D**). In transverse sections through the foregut, we confirmed localization of Aldh1a2 protein to the gut mesenchymal layer through which neural crest cells migrate, as well as in neural crest cells, using an antibody specific to zebrafish Aldh1a2. Signal was observed surrounding the gut endoderm, as marked by *sox17*:GFP (**Fig. 1E-E''**) and in neural crest visualized by *sox10*:GFP at 48 hpf (**Fig. 1F-F'',** arrows). Altogether, these results show that RA pathway components are expressed in the gut during enteric neural crest gut migration, consistent with possible functional roles therein.

Temporal addition of RA during colonization is sufficient to enhance enteric neuron numbers *in vivo*

Tissue culture studies have shown that RA can enhance enteric neural crest migration (Sato and Heuckeroth, 2008; Fu et al., 2010; Simkin et al., 2013), suggesting a role in enteric nervous system formation. To test the time during which RA plays a role in enteric neural crest migration, we tested the effects of exogenous application of RA during the migratory phase en route to and along the zebrafish gut. To this end, zebrafish embryos were incubated in 1 μ M RA or with DMSO alone, as a control, from 24-48 hpf or from 26-52 hpf. Migration of neural crest cells was visualized via expression of the pan neural crest marker *crestin* by *in situ* hybridization (**Fig. 2A-D**). When compared with control embryos, we observed an expansion of *crestin*$^{+}$ neural crest cells

along the vagal and anterior trunk level of the embryo in RA-treated embryos (**Fig. 2A,B**; arrows). Histological examination showed an expanded domain of *crestin*$^{+}$ cells localized near the vicinity of the foregut, when compared with control embryos (**Fig. 2C,D**; arrows).

As a secondary means of analyzing the distribution of neural crest cells, examination of the Tg(*sox10*:GFP) line revealed GFP^{+} cells surrounding the foregut in transverse sections at 52 hpf in control embryos (**Fig. 2E**), and an expansion of GFP^{+} neural crest cells near the foregut in RA-treated embryos (**Fig. 2F**; arrows). To test whether this early enhanced localization of neural crest cells later resulted in altered distribution of enteric neurons at larval stages, we performed whole mount immunochemistry with antibodies to the pan-neuronal marker Hu, as well as 5HT to identify serotonergic neurons in control and RA-treated larvae guts at 96 hpf. RA-treated larvae exhibited an increase in the total numbers of Hu^{+} enteric neurons along the gut, with an average of 106, compared with control larvae, which had an average of 87 Hu^{+} neurons (**Fig. 2G,H-H',I-I'**; p=.011). Similarly, RA-treated larvae exhibited increased numbers of 5HT^{+} neurons, with an average of 23, compared with control larvae, which had an average of 19 5HT^{+} neurons along the length of the gut (**Fig. 2G,H-H'',I-I''**; p=.001). However, the percentages of 5HT neurons were similar between control (21.8% 5HT^{+} neurons) and RA-treated (21.7% 5HT^{+} neurons) larvae indicating that RA addition increased the overall numbers of neurons. Collectively, these experiments suggest that addition of RA at the time when enteric neural crest cells invade and initiate migration along the rostrocaudal extent of the gut is sufficient to enhance the numbers of enteric precursors that subsequently leads to an increase in the numbers of enteric neurons *in vivo*.

Loss of RA during gut invasion prevents caudal colonization of the gut by enteric neural crest

In order to test the role of RA during early ENS development, we examined the effects of inhibiting RA pathway activity on the progression of enteric neural crest cell migration along the gut. Importantly, we inhibited RA signaling after 24 hpf to avoid early effects of RA on embryonic patterning and focus on its temporal role during ENS development. To this end, zebrafish embryos were treated with 10 μM DEAB (N,N-diethylaminobenzaldehyde), an aldehyde dehydrogenase inhibitor (Morgan et al., 2015), or DMSO for control, from 24-52 or 24-72 hpf. Such DEAB treatment did not result in global defects in neural crest localization at cranial or trunk levels, as assayed by examining the neural crest marker *crestin* in DEAB treated and control embryos at 52 hpf (**Fig. 3A,B;** arrows), nor did it alter the differentiation of neural crest-derived melanophores (**Fig. 3L**).

At 72 hpf, the localization of *crestin*$^{+}$ neural crest cells was evident within the hindgut in control larvae, while neural crest cells in DEAB treated larvae were restricted to the foregut (**Fig. 3C,D**; arrowhead), indicating delayed migration. To investigate the effects of RA inhibition on enteric neural crest localization along the gut in live larvae, we utilized the Tg(*-8.3phox2bb*:Kaede) line, which expresses the fluorescent protein Kaede under control of a 8.3 kilobase (kb) *phox2bb* enhancer (Harrison et al., 2014), expressed in enteric neuronal precursors and differentiated neurons. The results showed that DEAB treated larvae exhibited delayed enteric neural crest gut colonization. Whereas control larvae contained enteric neural crest at the level of the hindgut at 72 hpf, enteric neural crest cells were restricted to the foregut of DEAB treated larvae (**Fig. 3E,F**).

To assess possible effects of RA depletion of mesodermal tissue integrity along the gut, we examined larvae from the *TgBAC(hand2:GFP)* line (Yin et al., 2010) which labels gut mesenchyme along the gut tube. Using confocal z-stack imaging, we found no difference between control and DEAB-treatment in the anterior-posterior presence of gut mesenchyme in live larvae (**Fig. 3G,H**), demonstrating that gut mesodermal tissue is present along the gut tube following temporal reduction of RA.

Next, we investigated whether the delay in neural crest colonization of the gut after RA loss might be due to a reduction in the number of neural crest cells. To this end, we quantified numbers of neural crest cells along and near the foregut in transverse cryosections. Interestingly, DEAB treated *sox10*:GFP^{+} larvae did not exhibit a decrease in the number of neural crest cells with direct gut contact at 52 hpf, compared with controls (**Fig. 3I-K;** white arrows). However the number of *sox10*:GFP^{+} neural crest in the ventral mesenchyme surrounding the gut was increased (**Fig. 3I-K;** yellow arrows). These results suggest that neural crest cells accumulate in the vicinity of the foregut, but then fail to migrate along the gut following temporal loss of RA.

To confirm the effects of loss of RA on enteric development using an additional approach, we utilized the transgenic line Tg(*hsp70*:dnRAR-GFP) (Kikuchi et al., 2011), which expresses a dominant negative zebrafish Retinoic acid receptor, Raraa-GFP, under control of the heat shock promoter *hsp70*. Tg(*hsp70*:dnRAR-GFP)$^{-/+}$ embryos were subjected to a single one-hour heat shock at 24 hpf and allowed to to develop to 48-52 hpf. Heat shock control embryos (GFP^{-}) and heat shock-positive embryos (GFP^{+}) were analyzed by *in situ* hybridization against *crestin* (**Fig. S1**). Although *crestin* localization was not altered in the cranial or trunk neural crest regions (**Fig. S1A,B**), we observed a significant delay in enteric neural crest progression along the foregut in the

dnRAR embryos. When control embryos were examined in dorsal view, *crestin*$^{+}$ neural crest cells were present as two chains emanating from the post-otic vagal regions and migrating along the foregut, just past the level of the fin buds (**Fig. S1A';** arrows). In contrast, the foregut was just beginning to be colonized by neural crest in dnRAR-GFP^{+} embryos, with neural crest chains evident rostral to the level of the fin buds (**Fig. S1B';** arrows).

To examine enteric neural crest cell localization along the gut, Tg(*hsp70*:dnRAR-GFP) fish were crossed with Tg(*sox10*:mRFP) fish and mRFP^{+} progeny were heat shocked at 24 hpf and allowed to develop until 52 hpf. The front of enteric neural crest migratory chains was directly visualized by live confocal microscopy along the gut in GFP^{-} and GFP^{+} embryos as depicted in **Fig. S1C**. In control embryos, *sox10*:mRFP^{+} neural crest cells were present as a smooth, collective chain along the level of the midgut (**Fig. S1D,E**). By contrast, in dnRAR-GFP^{+} embryos, the enteric neural crest front was delayed in the foregut and appeared less organized and more dispersed, although they still remained in a migratory chain (**Fig. S1F,G**). These observations suggest that dampening RA pathway activity during the gut invasion stage is sufficient to delay migration of enteric neural crest cells along the gut *in vivo*. These results phenocopy the observations with DEAB treatment, leading to gut colonization defects (**Fig. 3**), consistent with a model in which RA is temporally required for the efficient migration of enteric neural crest along the foregut and midgut *in vivo*.

Loss of RA leads to stalled, disorganized migration of enteric neural crest along the foregut *in vivo*

To test the hypothesis that RA is required for the sustained and directed migration of enteric neural crest along the foregut, DMSO and DEAB treated *sox10*:mRFP^{+} larvae were live imaged during the second day of development using confocal time-lapse microscopy, as shown in **Fig. 4A**. In particular, we focused on the migratory front of the enteric neural crest chains in our time-lapse analysis. In control larvae, the *sox10*:mRFP^{+} enteric neural crest chain front was observed migrating caudally along the level of the midgut in a smooth, collective chain (**Fig. 4B,B', Movie 1**). In contrast, the DEAB treated *sox10*:mRFP^{+} enteric neural crest chain front was detected more rostrally along the foregut; although initially in a chain, the cells failed to progress caudally along the gut. Instead, enteric crest cells began to detach from one another at both the leading edge and along the trailing edge of the chain (**Fig. 4C,C';** arrows**, Movie 2**). Interestingly, not only did cells detach from one another, but they also began turning away from the chain both dorsally and ventrally (**Fig. 4C,C'**; arrows). Confirming the lack of progress along the gut, cell tracking analysis to follow leading cells over the course of 3 hours showed that control enteric neural crest cells collectively migrate caudally, while DEAB treated enteric crest fail to progress along the gut (**Fig. 4D,E**). Strikingly, the migratory chain front in DEAB treated larvae dissociated later at 72 hpf, when compared with controls (**Fig. 4F**). These data demonstrate that loss of RA as enteric neural crest migrate along the foregut leads to adverse consequences on neural crest migratory progress and the catastrophic loss of enteric neural crest chain integrity—leading to loss of directed chain migration along the gut (**Fig. 4G**). These results reveal a novel mechanism by which RA modulates enteric neural crest chain migration and suggest that RA is temporally required to ensure collective migration of the enteric neural crest chain along the foregut *in vivo*.

Temporal loss of RA does not affect enteric neuron differentiation, but leads to cell death and subsequent intestinal aganglionosis

We next examined if loss of RA, in addition to affecting migration, might have an effect on enteric neuron differentiation. During normal development, enteric neural crest cells migrate to the caudal end of the hindgut by ~72 hpf and begin to terminally differentiate into distinct enteric neuronal subtypes thereafter (Olsson et al., 2008; Olden et al., 2008; Uyttebroek et al., 2010; Taylor et al., 2016; Heanue et al., 2016). To investigate whether DEAB-treatment resulted in loss of differentiated neurons along the foregut, larvae were processed for whole mount immunochemistry using antibodies against Hu for differentiated neuronal cell bodies, acetylated tubulin for axons, or the neurotransmitter serotonin (5HT). In control larvae, Hu^+, $5HT^+$ and acetylated $tubulin^+$ neurons and axons were detected along the entire foregut (**Fig. 5A,C;** arrows; **Movie 3**); however in DEAB treated larvae, neurons were generally missing (**Fig. 5B,D; Movie 4**). Only one small cluster of ~3 neurons in the foregut of one DEAB treated larval fish was detected (**Fig. 5B;** arrow), indicating that temporal loss of RA results in intestinal aganglionosis.

During enteric neurogenesis in zebrafish, the first Hu^+ neurons are detected between ~52-54 hpf along the foregut (Olsson et al. 2008; Olden et al. 2008; Taylor et al. 2016). To determine if DEAB treatment alters the production of enteric neurons along the foregut at 52 hpf, and thus the initiation of enteric differentiation, *-8.3phox2bb*:$kaede^+$/Hu^+ neurons were examined in transverse section using immunohistochemistry in control and DEAB treated larvae. In control larvae, there was an average of 5.25 -

8.3phox2bb:$kaede^+$ enteric progenitors along the left and right sides of the foregut, of

which an average of 1.5 were Hu$^+$ (**Fig. 6A-A'', C, D**), 28.5% of the Kaede$^+$ cells. In DEAB treated larvae, an average of 13 *-8.3phox2bb*:kaede$^+$ enteric progenitors was detected; however they were distributed adjacent to the gut and around the ventral mesenchyme (**Fig. 6B-B''**, arrows) rather than in the foregut, in agreement with our previous finding using the *sox10*:GFP line (**Fig. 3K-M**). Among the *-8.3phox2bb*:kaede$^+$ enteric progenitors in DEAB treated larvae, an average of 6 were Hu$^+$(**Fig. 6D**), 46.2% of the Kaede$^+$ cells, demonstrating an overall increase in the number and proportion of neurons present.

The above results show that neurons differentiate properly in DEAB treated embryos and in fact are increased in number in the foregut when compared with controls. However, at later stages, neurons are missing. A possible explanation is that enteric neurons fail to survive after differentiation. To test this possibility, we performed immunostaining against activated-Caspase3 in control and DEAB- treated larvae at 70 hpf. As expected, in larvae examined in whole mount using confocal z-stack imaging, we observed elevated cell death within the enteric neural crest after loss of RA compared with controls (**Fig. 6E-E'',F-F'', Movie 5, Movie 6**). As secondary confirmation, we used immunohistochemistry on transverse sections through the foregut to examine the presence of apoptotic cells. The results confirm the presence of Caspase3$^+$ neural crest cells near the gut and in surrounding ventral mesencyhme, compared with controls (**Fig. 6G-G'', H-H''; arrows**). These observations indicate that enteric cells were undergoing cell death by this point, leading to a paucity of enteric neurons.

Collectively, these data demonstrate that temporal loss of RA results in accumulation of enteric neuronal progenitors along the foregut, which is later accompanied by cell death and a dramatic loss of enteric neurons resulting in HSCR-like

intestinal aganglionosis. Taken together with cell migration defects noted in Figs. 3, 4 and 5, these results reveal a previously unrecognized stage-dependent role for RA during the ontogeny of enteric neuron formation along the gut *in vivo*.

The transcription factor Meis3 functions downstream of RA in the neural crest to affect colonization of the gut

Next, we asked what transcriptional regulatory events might function downstream of RA signaling to regulate enteric colonization. One candidate is the transcription factor Meis3, a known RA-target gene in the zebrafish mesoderm (Waxman et al., 2008). We previously showed that its reduction resulted in colonic aganglionosis due to inefficient migration of enteric neural crest cells along the gut (Uribe and Bronner, 2015). To determine if *meis3* expression was altered following modulation of RA, we performed *in situ* hybridization after either temporal DEAB treatment, heat shock in *hsp70*:dnRAR-GFP embryos or exogenous RA treatment (**Fig. 7**). The results show that expression of *meis3* was missing in the vagal region and diminished in the foregut of DEAB treated embryos, compared with controls as viewed in whole mount (**Fig. 7A,B**; arrow). Similarly, following heat shock attenuation, the expression of *meis3* was restricted to a smaller domain along the foregut of GFP^+ embryos, when compared with heat shock controls, (**Fig. 7C,D;** arrowheads). Conversely, RA-treated embryos displayed an expansion of *meis3* expression within the foregut (**Fig. 7F**; arrow) as well as a rostral expansion in the hindbrain (**Fig. 7F**; bracket). By contrast, *meis3* expression in control embryos was restricted to the vagal-level hindbrain and foregut (**Fig. 7E**; bracket). These data demonstrate that *meis3* expression is altered following modulation of RA levels, suggesting that *meis3* may lie functionally downstream of RA.

To directly test a possible epistatic relationship between RA and Meis3 in enteric colonization, we asked whether ectopic expression of *meis3* was sufficient to rescue gut colonization and enteric neuronal differentiation following temporal loss of RA. To this end, *-8.3phox2bb*:Kaede embryos were injected with 25 or 40 pg of *meis3* mRNA at the 1-cell stage, developed until 24 hpf and incubated in 10μM DEAB, or DMSO for control, until 73 hpf. To assay for possible differences between enteric gut colonization and differentiation, whole mount immunochemistry was performed to detect the presence of *-8.3phox2bb*:Kaede^{+}/Hu^{+} neurons along the gut. The number of embryos from each condition exhibiting "normal colonization" (full gut), "partial colonization" (up to level of midgut) or "no colonization" (loss of neurons along whole gut) were scored. Control larvae possessed enteric neurons along the entire length of the gut (**Fig. 8A**), with 100% exhibiting normal colonization (**Fig. 8I**). Injection of *meis3* alone, at 25 pg (**Fig. S2**) and at 40 pg (**Fig. 8B**) had no effect on enteric neuron distribution along the gut, with 100% of larvae displaying normal colonization (**Fig. 8I**). In contrast, DEAB treated larvae exhibited neuronal loss along the entire length of the gut (**Fig. 8E**), with 100% of larvae exhibiting no colonization (**Fig. 8I**), consistent with our earlier experiments (**Fig. 3,5**). Injection of *meis3* mRNA together with DEAB-treatment led to a rescue in enteric neuron localization through the midgut (partial colonization) in ~67% of injected larvae (**Fig. 8F,I; Fig. S2)**.

To determine whether *meis3* functions downstream of RA specifically in the neural crest, rather than in the mesenchyme, we ectopically expressed *meis3* within neural crest by creating a construct *sox10:meis3-P2A-mcherry*. Its effects were compared with the control construct*, sox10:turq-P2A-mcherry*, which expresses the fluorophore Turquoise2. Injection of the control and *meis3* constructs were performed as

schematized in **Fig. 9A**. Embryos exhibiting mosaic mCherry^{+} expression in vagal neural crest cells at 24 hpf were sorted (**Fig. 9B,C**) and incubated in either DMSO, for control, or DEAB until 75 hpf. Control larvae expressing the control or *meis3* construct had Hu^{+} enteric neurons along all levels of the gut (**Fig. 9D,E**). In contrast, DEAB treated larvae expressing the control construct, *sox10:turq-P2A-mcherry,* displayed little or no colonization, with the exception of a single neuron (**Fig. 9F,H,** arrow). Conversely, DEAB treated larvae expressing the construct *sox10:meis3-P2A-mcherry* contained Hu^{+} enteric neurons in a mosaic manner throughout the gut at all levels (**Fig. 9G,I**; yellow arrows). These results show that ectopic expression of *meis3* within neural crest is sufficient to partially rescue colonization of the gut following RA loss, confirming that *meis3* functions downstream of RA signaling in the neural crest to affect enteric colonization of the gut *in vivo*.

Ectopic *ret* expression is sufficient to rescue gut colonization after RA loss

Another factor known to be important for ENS development is the receptor tyrosine kinase, RET, where its loss in both mouse and zebrafish leads to the catastrophic death of vagal neural crest prior to gut entry (Natarajan et al., 2002; Pachnis et al., 1998; Jain et al., 2004; Heanue et al., 2008). In avian explant cultures, RA has been shown to induce the expression of *Ret* in vagal neural crest cells (Simkin et al., 2013). To examine whether ectopic expression of *ret* alone or in combination with *meis3*, was sufficient to rescue gut colonization following RA attenuation, we assayed enteric neuron localization along the gut following injection of *ret*, or *ret* co-injected with *meis3,* in DMSO or DEAB treated larvae. Ectopic expression of *ret* (**Fig. 8C**), or *ret* plus *meis3* (**Fig. 8D**), did not affect colonization of the gut, with 100% of injected larvae exhibiting

normal colonization (**Fig. 8I**). In contrast, injection of *ret*, or *ret* plus *meis3*, in DEAB treated embryos led to rescue of enteric neuron localization through the midgut. Approximately 54% of *ret* injected larvae and 75% of *ret* + *meis3* injected larvae displayed colonization caudally to the midgut (**Fig. 8G,H,I**). These data show that *ret* and/or *meis3* were sufficient to rescue enteric colonization following temporal DEAB treatment. Moreover, their co-expression increases the percentage of larvae exhibiting midgut colonization after loss of RA (54% versus 75%).

Quantification of cell number along the rescued larval guts revealed that expression of *meis3*, *ret*, or *meis3* + *ret* was sufficient to partially rescue enteric neuron number following loss of RA (**Fig. 8J**). Whereas control larvae exhibited an average of 81.5 neurons, DEAB treated larvae exhibited an average of less than one neuron, 0.75 (**Fig. 8J**, $p<.0001$). In contrast, DEAB treated larvae expressing *meis3* contained an average of 20.75 neurons ($p<.0001$), larvae expressing *ret* contained an average of 22.75 neurons, and larvae expressing *meis3* + *ret* contained 26.25 neurons ($p<.001$) (**Fig. 8J**). Neuron number was slightly increased when comparing larvae expressing *meis3* versus *meis3* + *ret* following DEAB treatment, but not significantly (20.75 vs. 26.25, $p=.1373$).

Collectively, these epistatic rescue data show that *meis3* and *ret* function downstream of the RA signaling pathway during early ENS formation, thus expanding the known signaling network underlying enteric nervous system formation.

RA affects colonization of the gut during early foregut invasion stages

Finally, we examined the precise time period during which RA functions by treating embryos for discrete time windows: from 28-36, 36-48 or 48-73 hpf with DMSO

or DEAB. Embryos were allowed to develop to 73 hpf to assay for the presence of Hu^+ neurons along the gut. Control embryos displayed neurons along all levels of the gut (**Fig. 10A, E**), with 100% exhibiting normal colonization. In comparison, larvae treated from 48-73 hpf also exhibited neurons along all levels of the gut (**Fig. 10D,E**), with 95% of larvae exhibiting normal colonization. Thus, the presence of RA during later phases of enteric migration is not required for colonization. In contrast, treatment with DEAB from 28-36 hpf resulted in loss of colonization along the whole gut in 76% of larvae, with the other 24% exhibiting partial colonization (**Fig. 10B,E**). Treatment from 36-48 hpf lead to 64% of larvae with partial colonization of the gut, 17% with no colonization, and 19% appearing largely normal (**Fig. 10C,E**). Taken together, these time-course experiments indicate that RA is required during the early neural crest foregut invasion stage plus subsequent migration of neural crest cells along the foregut, but is less important thereafter. These results are concordant with our previous results suggesting that RA is critical for gut invasion and neural crest migration along the foregut (**Fig. 3, 4, 5**), playing a stage-specific role in ENS formation.

Discussion

We have identified a critical role for retinoic acid in orchestrating the collective chain migration and survival of enteric neural crest cells along the developing gut *in vivo*. Using zebrafish as a model system, our findings reveal that RA functions in a temporally important manner; when enteric neural crest cells migrate into and along the foregut, to modulate the efficient collective chain migration of enteric neural crest cells to ensure complete colonization of the gut (**Fig. 10F**). Specifically, we found that loss of RA during the migratory phase caused enteric neuronal progenitors to stall in their migratory

progress and accumulate near the foregut, subsequently dissociating from collective chains into detached cells (Fig. 3, 4, 6). Although following RA reduction we observed no effect on ability to differentiate into enteric neurons, they subsequently underwent apoptosis, leading to intestinal aganglionosis in which the gut lacked nearly all neurons (Fig. 5, 6). Conversely, application of exogenous RA during enteric neural crest migration enhanced the number of enteric neural crest and increased the total number of differentiated neurons along the gut *in vivo* (Fig. 2). Moreover, we find that the transcription factor Meis3, as well as the receptor RET, can partially rescue the enteric colonization defects caused by loss of RA (Fig. 8), thus identifying molecular effectors that influence ENS development downstream of RA signaling. Cumulatively, these results provide novel insights into the cellular and molecular mechanisms by which the early ENS is created and suggest that Vitamin A/RA-coupled susceptibility to HSCR may occur precisely within a narrow time window during embryonic development.

Our results are consistent with previous literature suggesting that retinoid availability and abundance during ENS development can lead to adverse consequences on ENS formation. For example, it was found that depletion of endogenous RA (via knockout of *Aldh1a2*) caused a failure in ENS formation due to the severe loss of vagal neural crest cells prior to gut entry (Neiderreither et al., 2003), achieved by rescuing early embryonic lethality in *Aldh1a2*$^{-/-}$ mice with RA. However, the partially rescued embryos exhibited a myriad of other embryonic defects, making the precise role of RA in the ENS difficult to parse. Similarly, dietary Vitamin A (retinol) deficiency, coupled with genetic predisposition, has been shown to cause HSCR in a mouse model (Fu et al. 2010). In this study, the authors showed that while *Rbp4*$^{-/-}$ mice displayed largely normal ENS development, added restriction of maternal dietary Vitamin A during ENS development

depleted retinoid levels and led to colonic aganglionosis in more than half of the mice analyzed. These results suggest that optimal levels of Vitamin A are necessary for gut colonization in genetically predisposed mice; however how Vitamin A deficiency functionally affects enteric neural crest migration, proliferation or differentiation *in vivo* was not fully addressed. *In vitro* and gut explant studies further support a role for RA in enteric neural crest migration, proliferation and differentiation. For example, incubation in excess RA caused expansion of isolated enteric neural crest cells cultured from E12.5 mice, a time point in which enteric neural crest have migrated into the colon, and an increase in their neuronal differentiation (Sato and Heuckeroth, 2008). In slice cultures of E12.5 mid-small gut, application of a RAR inhibitor, BMS493, reduced net migration distance traveled by enteric neural crest in response to a GDNF gradient and reduced the density of enteric neural crest along colon tissue in gut explant, contributing to colonic hypoganglionosis (Fu et al., 2010). Additionally, RA application to quail vagal neural crest cells prior to and during gut entry conferred ability to migrate efficiently in chains along aneural gut explant tissue (Simkin et al., 2013).

The present work in zebrafish extends these findings in a system where it is possible to examine enteric neural crest development *in vivo*, in a temporally defined manner. We discovered that blockade or enhancement of RA signaling, using pharmacological (DEAB and RA) and genetic means (*hsp70*:dnRAR), during enteric neural crest migration stages resulted in altered enteric neural crest development in the foregut: exogenous RA application led to increased enteric neuron numbers during larval stages, whereas temporal attenuation of RA caused loss of colonization (aganglionosis) of the gut. Live time-lapse confocal analysis of migrating enteric neural crest cells revealed compromised chain migration and integrity, leading to the accumulation of

enteric crest within the foregut. Although this had no effect on enteric neurogenesis, subsequently enteric neuronal progenitors became ectopically localized in the ventral mesenchyme and underwent apoptosis that ultimately led to intestinal aganglionosis.

Of particular interest, we identified Meis3 as a functional player downstream of RA in the developing ENS. Meis3 is a known RA response gene in the zebrafish lateral plate mesoderm (Van der Velden et al., 2012; Waxman et al., 2008), in the neural ectoderm (Kudoh et al., 2002) and in developing mouse limbs (Qin et al., 2002). Meis3 has also been discovered to function with RA to pattern the early frog hindbrain (Dibner et al., 2001). We showed that loss of Meis3 results in decreased enteric precursor migration along the gut that leads to colonic aganglionosis (Uribe and Bronner, 2015). The present results suggest that Meis3 functions downstream of RA to influence enteric neural crest cell migration and development. Our results show that Meis3 is down-regulated after loss of RA and upregulated with excess RA. Moreover, ectopic expression of *meis3* within neural crest partially rescues gut colonization after loss of RA, suggesting that *meis3* is downstream of RA in the neural crest (Fig. 9). These experiments demonstrate a vital role for *meis3* as a RA effector important for enteric colonization. To date, this is the first report to functionally describe a transcription factor downstream of RA to influence ENS development in any system.

In addition to *meis3,* our data suggest that RA functions to affect the RET-Gfra1-Gdnf pathway. Gfra1 is a glycosyl phosphatidylinositol (GPI) attached receptor expressed on enteric neural crest cells along with Ret (Worley et al., 2000; Airaksinen and Saarma, 2002; Natarajan et al., 2002; Shepherd et al., 2004). GDNF is expressed in the gut mesenchyme that enteric neural crest cells migrate through (Worley et al., 2000; Natarajan et al. 2002; Reichenbach et al., 2008). Following loss of *Ret* or *GDNF*, vagal

neural crest cells undergo apoptosis before and as they enter the foregut environment, leading to loss of enteric progenitors (Schuchardt et al., 1994; Sanchez et al., 1996; Moore et al., 1996; Pichel et al., 1996). Notably, application of RA to the early neural tube in chicken embryos (Robertson and Mason, 1995) and in culture (Simkin et al., 2013) expands the domain and/or upregulates the expression of *Ret*. Consistent with this, we find that ectopic expression of *ret* mRNA is sufficient to rescue midgut colonization following loss of RA and to partially rescue enteric neuron number (Fig. 8), suggesting that RET is downstream of the RA during ENS development *in vivo*. In addition, ectopic expression of *ret* plus *meis3* increased the percentage of embryos that exhibited midgut colonization rescue following DEAB treatment (75%) compared with *meis3* alone (67%) or *ret* alone (54%), suggesting that *ret* and *meis3* may function together to affect caudal colonization of the gut downstream of RA signaling. In contrast, *ret* plus *meis3* did not significantly enhance the number of enteric neurons following DEAB treatment (Fig. 8J) compared with *meis3* alone or *ret* alone. This suggests that the extent to which cells have migrated caudally may be separable from the total numbers of enteric neurons present in the whole gut, with respect to *meis3* and *ret*. In light of these data, our results suggest that *ret* and *meis3* may act in a shared pathway to influence enteric neural crest migration, but not total cell number, along the gut.

Ret mutations are known to be a major cause of HSCR in humans and the conservation of this function has been demonstrated in numerous model organisms, such as mouse and zebrafish (Natarajan et al., 2002; Pachnis et al., 1998; Jain et al., 2004; Heanue et al., 2008). Due to its significance in the etiology of HSCR, much research has focused on elucidating the molecular mechanisms underlying its function, regulation and spatial distribution during development. Recently, a study examining the conserved

regulatory enhancers that modulate the expression of *Ret* in humans, and often mutated in human HSCR patients, has identified that Rarb directly binds an enhancer element, RET -7, in conjunction with two other enhancers, RET -5.5 and RET +3, bound by the transcription factors Gata2 and Sox10, respectively (Chatterjee et al., 2016). This study implicates RA signaling in modulation of *Ret* expression via *Rarb*, therefore suggesting that RA may be functionally important for development of the ENS in humans and the etiology of HSCR.

Examination of gut mesenchyme using a BAC transgenic reporter of *hand2* expression revealed no qualitative difference in gut mesenchyme tissue along the anterior-posterior length of the gut tube in live larvae treated with DEAB versus control (Fig. 3). However, we have not ruled out the possibility that differentiation of the intestinal mesenchyme may be altered following RA inhibition. For example, following loss of *hand2* in zebrafish, smooth muscle fails to differentiate, coincident with a reduction of enteric neuron colonization and differentiation along the gut (Reichenbach et al., 2008). Nonetheless, Seiler et al. discovered that differentiation of smooth muscle in zebrafish occurred after enteric neuron terminal differentiation (Seiler et al., 2010), suggesting that enteric colonization and differentiation does not depend upon differentiated gut mesenchyme. Corroborating these data, previous studies in amniotes have shown that differentiation of foregut (stomach) mesenchyme depends upon and follows the arrival of enteric neural crest cells (Faure et al., 2016; Bourret et al., 2017); loss of enteric neural crest cells via tissue-specific ablation impairs the Notch signaling pathway in stomach mesenchyme and perturbs smooth muscle development (Faure et al., 2016). Thus, it may be difficult to parse whether effects on the mesenchyme are direct or indirect via alterations to the neural crest.

Our live imaging and perturbation results *in vivo* suggest that retinoid depletion during enteric migratory phases can lead to adverse consequences on enteric neural crest migration and chain formation during ENS development. In the gut environment, RA pathway components are expressed in the mesenchyme, within the epithelium and in neural crest cells. Between E12.5 and E14.5 in the mouse gut, pathway components involved in RA response are present, such as *Rara*, *Rarg* and *Rxrg*, as well as those involved in its synthesis and degradation, such as *Aldh1a1-3* and *Cyp26a1* (Sato and Heuckeroth, 2008). *Aldh1a2* is detected within the gut mesenchyme, in agreement with our findings in zebrafish tissue (Fig. 1). Live time-lapse analysis shows that chains of enteric neural crest collectively migrate caudally in a precise and organized manner along the gut tube (Fig. 4) (Harrison et al., 2014; Uribe and Bronner, 2015). By contrast, we discovered that RA inhibition stalled enteric neural crest migration into and along the foregut and cells along the leading and trailing edge veered dorsally and ventrally, but did not progress caudally. By 72 hpf, the enteric neural crest chain dissociated along the foregut, when compared with control (Fig. 4). These results suggest that RA is necessary for the propelled caudal advance of enteric neural crest along the gut and implicate it in promoting efficient chain migration. Our results in live embryos are consistent with previous findings in explant culture, where application of RA to vagal neural crest was sufficient to enhance chain migration and RA inhibition disrupted chain formation of enteric crest in aneural gut tissue (Simkin et al., 2013). RA also has been shown to be important for the formation of lamellapodia on enteric progenitors and to prevent accumulation of the phosphatase PTEN within leading edge cells (Fu et al., 2010) by modulation of the Rac1-Rho signaling pathway, which influences actin-cytoskeletal dynamics (Fukuda et al., 2002; Hall, 2005; Vohra et al., 2007). Therefore, it

598 is possible that localization of polarized intracellular effectors of cell migration is affected
599 following loss of RA.

600 In mouse gut explants, enteric neural crest cells migrate as a web of chains
601 caudally along the growing gut tube (Young et al., 2014), with solitary cells roaming
602 chaotically in a random walk near the vicinity of the chains. Net advancement of the
603 wave front occurred more rapidly than the trailing edge ensuring colonization of the
604 hindgut. In contrast, in our time-lapse movies of the zebrafish gut, we did not detect
605 evidence for solitary enteric neural crest near the collective chain. However, following RA
606 inhibition, we did identify solitary enteric neural crest in the ventral mesenchyme
607 surrounding the gut (Fig. 4, 6). It could be that RA normally inhibits enteric neural crest
608 dispersal along the gut and maintains the sole presence of a collective chain. Zebrafish
609 enteric neural crest, therefore, may represent a simplified method of chain migration in
610 response to cues and provides a tractable model to study detailed mechanisms of this
611 particular behavior *in vivo*.

612 Taken together, our results are the first *in vivo* study to show a temporal
613 requirement for Retinoic Acid in enteric neural crest migration *in vivo* in any species. The
614 use of zebrafish as a model further enables us to examine the effects of RA loss using
615 live imaging. We find that enteric neurogenesis commences in the absence of RA, but
616 then is followed by neuronal death. These data suggest a model in which vagal neural
617 crest cells residing within the post-otic vagal region respond to local RA signaling cues
618 and commence migration toward the foregut entrance. Once within the gut
619 mesenchyme, enteric neural crest cells are exposed to RA and Meis3-RET signaling as
620 they migrate caudally in response to a GDNF gradient. Sustained RA signaling and its
621 downstream activation of Meis3 ensures collective enteric neural crest chain integrity as

they navigate through the gut mesenchyme and ensures the survival of nascent enteric neurons (Fig, 10F). Future studies focused on whether RA pathway components function to affect the expression of Ret and other HSCR-associated genes directly, or via a conserved regulatory element, using a combination of mouse and zebrafish models, will greatly enhance our understanding of the molecular and genetic mechanisms underlying construction of the ENS *in vivo*.

Materials and Methods

Zebrafish Maintenance and lines

Zebrafish (*danio rerio*) were maintained at 28.5°C on a 13-hour light/11 hour dark cycle. Animals were treated in accordance with California Institute of Technology IACUC provisions. The following zebrafish lines used include: Wild-type AB (Zebrafish International Resource Center), Tg(-*4.9sox10*:GFP; *ba2Tg*) (Carney et al., 2006), Tg(*sox10*:mRFP; *vu234Tg*) (Kucenas et al., 2008), Tg(-*8.3phox2bb*:Kaede; *em2Tg*) (Harrison et al., 2014), TgBAC(*hand2*:GFP; *pd24Tg*) (Yin et al., 2010), Tg(*sox17*:GFP; *s870Tg*) (Sakaguchi et al., 2006) and Tg(*hsp70*:dnraraa-GFP; *pd18Tg*) (Kikuchi et al. 2011).

Pharmacological treatments

Embryos were de-chorionated and incubated in 1 µM Retinoic Acid (RA) (190269 MP Biomedicals) or 10 µM N,N-diethylaminobenzaldehyde (DEAB) (D86256 Sigma Aldrich) from 24-48 hpf onwards, depending on experiment as described in the Results. Embryos were then either removed from treatment and immediately fixed and processed for

downstream experiments or allowed to recover in egg water depending upon experimental endpoint as described in the Results section.

Rescue construct cloning, mRNA synthesis and microinjections

The coding sequence of *ret* was amplified using the following primers from 35 hpf cDNA: forward 5' GGCTCCTTTCGCTCGAATCA 3', reverse 5' GCCGTTAGCACAATCACAGC 3', ligated into pGEM-Teasy vector (Promega), and sequence verified. *ret* cDNA was then subcloned into pCS2^{+} vector to create pCS2-*ret*, which was linearized with ClaI and used as template to generate *ret* capped mRNA using the T3 mMessage RNA synthesis kit (Ambion). pCS2-*meis3* (Uribe and Bronner, 2015) was linearized with NotI and used as a template to generate *meis3* capped mRNA with the Sp6 mMessage RNA synthesis kit (Ambion). Tg(-*8.3phox2bb*:Kaede) embryos were injected with 25 or 40 pg of *meis3* mRNA and/or 50 pg of *ret* mRNA at the one-cell stage. Injected embryos and uninjected controls were incubated in either DMSO or DEAB from 24-73 hpf and immediately fixed for anti-Hu, anti-Kaede immunohistochemistry as described below. The number of embryos from each condition exhibiting "normal colonization" (full gut), "partial colonization" (up to level of midgut) or "no colonization" (loss of neurons along whole gut) was counted and the percentages represented in bar graph format using Excel software (Microsoft).

For neural crest tissue-specific rescue experiments, the zebrafish *sox10* promoter (Carney et al., 2006) was subcloned into the Gateway 5' entry vector p5E, to create p5E-*sox10,* via HindIII/SpeI sites. The coding sequence of *meis3* with no stop codon was PCR amplified using the following primers, to add KpnI/SacII sites: 5' CGGGTACCATGGATAAGAGGTATGAG 3', 5'

CGCCGCGGTGTGGGCATGTATGTCAAG 3'. The construct pME-Turquoise (Turq) (Oehlers et al., 2014) was used as template to PCR amplify the coding sequence of the fluorophore Turq with no stop codon using the following primers, to add KpnI/SacII sites: 5' ATGGTACCCCATGGTGAGCAAGGGCG 3', 5' CGCCGCGGtCTTGTAGAGCTCGTCCAT 3'. The Gateway middle entry vector pME was PCR amplified to add KpnI/SacII sites with the following primers: 5' CGCCGCGGACCCAGCTTTCTTGTACA 3', 5' CGGGTACCGGGTCCCCAAACTCACCC 3', creating pME-KS. *meis3* no stop and *turq* no stop PCR fragments were then directionally cloned into pME-KS to create pME-*meis3* no stop and pME-*turq* no stop, respectively. For final construction reactions, p5E-*sox10*, pME-*meis3* no stop, or pME-*turq* no stop, and p3E-P2A-mCherry (Villefranc et al., 2013; addgene # 26031) was then used in a Gateway LR Clonase II plus reaction (Invitrogen) using the destination vector pDestTol2pA2 (Kwan et al., 2007) to create *pDest-Tol2-sox10-meis3-P2A-mcherry-pA2* and *pDest-Tol2-sox10-turq-P2A-mcherry-pA2*. Constructs were injected individually into the 1-cell stage embryo at 25 pg each, along with 30 pg of Tol2 transposase mRNA. Tol2 mRNA was created by linearizing the construct pCS2-transposase (Kwan et al., 2007) with Not1 and transcribing mRNA using the Sp6 mMessage RNA synthesis kit (Ambion). *pDest-sox10-meis3-P2A-mcherry-pA2* and *pDest-sox10-turq-P2A-mcherrypA2* injected embryos were sorted for mCherry signal at 24 hpf and incubated in DMSO or the inhibitor DEAB until 75 hpf, then accordingly fixed and subjected to anti-Hu immunohistochemistry to assay for neuronal colonization of the gut tube. Injection-rescue experiments were repeated using three biological replicates, with n=10 for each condition, therefore each replicate N=40; total N=120 across all three replicates.

in situ hybridization

Whole mount *in situ* hybridizations were performed essentially as described (Jowett and Lettice, 1994). The following cDNA constructs were used as templates to generate anti-sense probes: *meis3* (Rauch et al., 2003), *crestin* (Luo et al., 2001), *rbp5* (formerly *rbp1a*; cDNA #cb465, Zebrafish International Resource Center), *crabp2a* (cDNA #cb432, Zebrafish International Resource Center), and *aldh1a2* (Feng et al., 2010). Following *in situ* hybridization, embryos were processed into 75% glycerol and imaged whole-mount or incubated in 15% sucrose, embedded in 7.5% gelatin and cryosectioned for histological examination. Sections were imaged using a Zeiss Image.M2 Apoptome.2 microscope using the DIC image settings and a Plan-Apochromat/.8 20X objective. All images were processed and cropped using Acrobat Adobe Photoshop CS6 software.

Immunohistochemistry and image analysis

Larvae were fixed and prepared for immunohistochemistry as previously described (Uribe and Bronner, 2015). The following antibodies were used: rabbit anti-GFP 1:500 (Life Technologies, A-11122), goat anti-GFP 1:500 (Abcam, ab6673), mouse anti-pH3 1:500 (Abcam, ab14955), rabbit anti-Aldh1a2 1:500 (Genetex, GTX124302), rabbit anti-Kaede 1:250 (MBL International, PM102M), mouse anti-HuC/D 1:200 (Invitrogen), rabbit anti-Caspase3 1:500 (R&D Systems, AF835) or rabbit anti-5HT 1:1000 (Immunostar). The following secondary antibodies were used: Alexa Fluor Goat anti-Rabbit 488, Donkey anti-Goat 488, Goat anti-Rabbit 568 or Goat anti-Mouse 633 (Invitrogen) was used 1:700. DAPI and/or Alexa Fluor 568 Phalloidin (Invitrogen) were included with some secondary antibody incubations to visualize nuclei or F-actin, respectively, on cryosections. Whole mount embryos were processed into 75% glycerol prior to imaging.

Cryosections were imaged using a Zeiss Image.M2 Apoptome.2 microscope and a Plan-Apochromat/.95 korr 40× oil objective and whole-mount embryos were imaged with a Zeiss LSM 800 confocal laser-scanning microscope using a Plan-Apochromat/.8 20X objective and Zen software. For confocal images, z-stacks were acquired laterally along the gut encompassing the region where neural crest cells or enteric neurons were detected, with z-stack intervals ranging from 18-30 microns thick and slices acquired every 1-3 microns. Confocal images were processed and exported as maximum intensity projections using Imaris imaging software (Bitplane) in the form of .tif files and/or rendered as 3D rotation animations in .mp4 format to view whole z-stack tissue.. For cell counts on cryosections, cells were quantified in comparable axial locations along the foregut in control and DEAB treated larvae. For counts in whole-mount guts, neurons were counted from maximum intensity Z-stack projections. The average number of cells was depicted in bar graph format using Prism software (Graphpad). Statistical difference between two conditions was determined using Student's *t*-test analysis with Prism software (Graphpad). The significance threshold was set at .05. All final images were processed and cropped using Acrobat Adobe Photoshop CS6 software.

Heat shock experiments

Tg(*hsp70*:dnraraa-GFP)$^{+/-}$ fish were transferred from 28.5°C to 38°C preheated water at 24 hpf for one hour and then transferred back to 28.5°C to recover for 3 hours. Heat shocked embryos were then examined and sorted for GFP fluorescence, accordingly sorted into GFP^{-} and GFP^{+} groups, incubated until 48 or 52 hpf and processed for immediate downstream experiments.

Live imaging

Tg(*sox10*:mRFP), Tg(*phox2bb*:kaede) or TgBAC(*hand2*:GFP) larvae were anesthetized in low dose tricaine, embedded in 1% low melt agarose dissolved in egg water in a glass-bottom imaging chamber (Lab-Tek, chambered #1.0 Borosilicate) and imaged using a 20X Plan-Apochromate/ .8 objective, in a 28.5°C heated imaging chamber on a Zeiss LSM 800 confocal laser scanning microscope. For time-lapse analysis, control and DEAB treated larval fish were oriented laterally against the bottom of the imaging chamber and the foregut-midgut level of the gut was examined. Z-stacks ~30 microns thick, encompassing the area of gut where enteric neural crest chains were evident, were acquired every 10 minutes. Acquired time-lapse movies were exported as .mp4 files, time lapse stills were exported as .tif images and cell track analysis was used to manually track the first few cells of the enteric neural crest chain in control and DEAB treated larvae over the course of 3 hours using an Imaris imaging software system (Bitplane) in the Biological Imaging Facility (BIF), Caltech, Pasadena, Ca.

Author Contributions

R.A.U. and M.E.B designed the study; R.A.U. and S.S.H. performed experiments and collected data; R.A.U. and M.E.B. analyzed data, drafted the manuscript and obtained funding.

Acknowledgements

We thank Kenneth Poss, Stephanie Woo and Iain Shepherd for fish lines, the Zebrafish International Resource Center (ZIRC) for cDNA constructs, David Tobin for the pME-

Turquoise construct. We thank Yuwei Li for help with cell track analysis, Can Li, Wael El-Nachef, Kendrick Shen and Joanne Tan-Cabugao for technical assistance and David Mayorga for fish care. Confocal imaging and Imaris image analysis for this study was performed in the Biological Imaging Facility (BIF), Caltech. This work was funded by a Burroughs Wellcome Fund Postdoctoral Enrichment Program Award (PDEP) and a NIH National Research Service Award (NRSA) HD080343 to R.A.U.; by a Caltech Summer Undergraduate Research Fellowship (SURF) to S.S.H; by a NIH grant DE024157 and a fish facility grant from Beckman Institute, Caltech, to M.E.B. The authors declare no competing financial interests.

References:

Airaksinen, M.S. and Saarma, M. (2002). The GDNF family: signaling, biological functions and therapeutic value. Nat Rev Neurosci 3(5): 383-94.

Anderson, R.B., Stewart, A.L., Young, H.M., 2006. Phenotypes of neural-crest-derived cells in vagal and sacral pathways. Cell Tissue Res 323, 11-25.

Barber, T., Esteban-Pretel, G., Marin, M.P. and Timoneda, J. (2014). Vitamin A deficiency and alterations in the extracellular matrix. Nutrients 6 (11): 4984-5017.

Bergeron, K. F., D. W. Silversides and N. Pilon (2013). The developmental genetics of Hirschsprung's disease. Clin Genet 83(1): 15-22.

Bourret, A., Chauvet, N., de Santa Barbara, P. and Faure, S. (2017). Colonic mesenchyme differentiates into smooth muscle before its colonization by vagal enteric neural crest-derived cells in the chick embryo. Cell Tissue Res. 368(3):503-511.

Burns, A. J., D. Champeval and N. M. Le Douarin (2000). Sacral neural crest cells colonise aganglionic hindgut in vivo but fail to compensate for lack of enteric ganglia. Dev Biol 219(1): 30-43.

Carney, T.J., Dutton, K.A., Greenhill, E., Delfino-Machin, M., Dufourcq, P., Blader, P., Kelsh, R.N., 2006. A direct role for Sox10 in specification of neural crest-derived sensory neurons. Development 133, 4619-4630.

Chatterjee, S., Kapoor, A., Akiyama, J.A., Auer, D.R., Lee, D., Gabriel, S., Berrios, C., Pennachhio, L.A. and Chakravarti, A. (2016). Enhancer variants synergistically drive dysfunction of a gene regulatory network in Hirschsprung Disease. Cell 167: 355-68.

Dibner, C., S. Elias and D. Frank (2001). XMeis3 protein activity is required for proper hindbrain patterning in Xenopus laevis embryos. Development 128(18): 3415-3426.

Druckenbrod, N. R. and M. L. Epstein (2005). The pattern of neural crest advance in the cecum and colon. Developmental Biology 287(1): 125-133.

Dutton, K. A., A. Pauliny, S. S. Lopes, S. Elworthy, T. J. Carney, J. Rauch, R. Geisler, P. Haffter and R. N. Kelsh (2001). Zebrafish colourless encodes sox10 and specifies non-ectomesenchymal neural crest fates. Development 128(21): 4113-4125

804 Elworthy, S., J. P. Pinto, A. Pettifer, M. L. Cancela and R. N. Kelsh (2005). Phox2b
805 function in the enteric nervous system is conserved in zebrafish and is sox10-dependent.
806 Mech Dev 122(5): 659-669.
807 Epstein, M.L., Mikawa, T., Brown, A.M., McFarlin, D.R., 1994. Mapping the origin of the
808 avian enteric nervous system with a retroviral marker. Dev Dyn 201, 236-244.
809 Faure, S., McKey, J., Sagnol, S. and de Santa Barbara, P. (2015). Enteric neural crest
810 cells regulate vertebrate stomach patterning and differentiation. Development 142(2):331-
811 42.
812 Feng, L., Hernandez, R.E., Waxman, J.S., Yelon, D. and Moens, C.B. (2010). Dhrs3a
813 regulates retinoic acid biosynthesis through a feedback mechanism. Developmental
814 Biology 338(1):1-14.
815 Fu, M., Sato, Y., Lyons-Warren, A., Zhang, B., Kane, M.A., Napoli, J.L., Heuckeroth,
816 R.O., 2010. Vitamin A facilitates enteric nervous system precursor migration by reducing
817 Pten accumulation. Development 137, 631-640.
818 Fukuda, T., Kiuchi, K. and Takahashi, M. (2002). Novel mechanism of regulation of RAC
819 activity and lamellipodia formation by RET tyrosine kinase. Journ of Biol Chemistry 277:
820 19114-121.
821 Furness, J. B. (2006). The Enteric Nervous System, Blackwell Publishing, Inc.
822 Ganz, J., Melancon, E. and Eisen, J. (2016). Zebrafish as a model for understanding
823 enteric nervous system interactions in the developing intestinal tract. Methods Cell Biol
824 134: 139-64.
825 Green, S. A., Simoes-Costa, M. and Bronner, M.E. (2015). Evolution of vertebrates as
826 viewed from the crest. Nature 520(7548):474-82.
827 Hall, A. (2005). Rho GTPases and the control of cell behavior. Biochem Soc Trans 33:
828 891-95.
829 Harrison, C., Wabbersen, T. and Shepherd, I.T. (2014). In vivo visualization of the
830 development of the enteric nervous system using a Tg(-8.3phox2b:Kaede) transgenic
831 zebrafish. Genesis 52 (12): 985-90.
832 Heanue, T.A. and Pachnis, V. (2008). Ret isoform function and marker gene expression
833 in the enteric nervous system is conserved across diverse vertebrate species. Mech Dev
834 125(8): 687-99.
835 Heanue, T.A., Shepherd, I.T. and Burns, A.J. (2016). Enteric nervous system
836 development in avian and zebrafish models. Developmental Biology 417 (2): 129-38.
837 Jian, S., Naughton, C.K., Yang, M., Strickland, A., Vij, K., Encinas, M., Golden, J., Gupta,
838 A., Heuckeroth, R., Johnson, E.M. and Milbrandt, J. (2004). Mice expressing a dominant-
839 negative Ret mutation phenocopy human Hirschsprung disease and delineate a direct
840 role of Ret in spermatogenesis. Development 131(21): 5503-13.
841 Jowett, T. and L. Lettice (1994). Whole-mount in situ hybridizations on zebrafish embryos
842 using a mixture of digoxigenin- and fluorescein-labelled probes. Trends Genet 10(3): 73-
843 74.
844 Kapur, R.P. (1999). Early death of neural crest cells is responsible for total enteric
845 aganglionosis in Sox10(Dom)/Sox10(Dom) mouse embryos. Pediatr Dev Pathol 2(6):
846 559-569.
847 Kelsh, R.N. and Eisen, J. (2000). The zebrafish colourless gene regulates development
848 of non-ectomesenchymal neural crest derivatives. Development 127(3): 515-25.
849 Kikuchi, K., Holdway, J.E., Major, R.J., Blum, N., Dahn, R.D., Begemann, G., and Poss,
850 K.D. (2011). Retinoic Acid production by endocardium and epicardium is an injury
851 response essential for zebrafish heart regeneration. Dev. Cell 20(3): 397-404.

Knight, R.D., Nair, S., Nelson, S.S., Afshar, A., Javidan, Y., Geisler, R., Rauch, G.L. and Schilling, T.F. (2003). lockjaw encodes a zebrafish tfap2a required for early neural crest development. Development 130(23):5755-68.

Kucenas S., Takada N., Park H.C., Woodruff E., Broadie K., Appel B. (2008). CNS-derived glia ensheath peripheral nerves and mediate motor root development. *Nat Neurosci* 11:143–151.

Kudoh, T., Wilson, S.W., and Dawid, I.B. (2002) Distinct roles for Fgf, Wnt and retinoic acid in posteriorizing the neural ectoderm. Development ,129(18):4335-4346.

Kuo, B.R., Erickson, C.A., 2011. Vagal neural crest cell migratory behavior: a transition between the cranial and trunk crest. Dev Dyn 240, 2084-2100.

Kwan, K.M., Fujimoto, E., Grabher, C., Mangum, B.D., Hardy, M.E., Campbell, D.S., Parant, J.M., Yost, H.J., Kanki, J.P., and Chien, C.B. (2007) The Tol2kit: A multisite gateway-based construction kit for Tol2 transposon transgenesis constructs. Dev Dynamics. 236(11):3088-3099.

Lang, D., Chen, F., Milewski, R. et al. (2000). Pax3 is required for enteric ganglia formation and functions with Sox10 to modulate expression of c-ret. J Clin Invest 106(8):963-971.

Le Douarin, N.M., Teillet, M.A., 1973. The migration of neural crest cells to the wall of the digestive tract in avian embryo. J Embryol Exp Morphol 30, 31-48.

Luo, R., M. An, B. L. Arduini and P. D. Henion (2001). Specific pan-neural crest expression of zebrafish Crestin throughout embryonic development. Dev Dyn 220(2): 169-174.

Montero-Balaguer, M., M. R. Lang, S. W. Sachdev, C. Knappmeyer, R. A. Stewart, A. De La Guardia, A. K. Hatzopoulos and E. W. Knapik (2006). The mother superior mutation ablates foxd3 activity in neural crest progenitor cells and depletes neural crest derivatives in zebrafish. Dev Dyn 235(12): 3199-3212.

Moore, M.W., Klein, R.D., Farinas, I., Sauer, H., Armanini, M., Phillips, H., Reichardt, L.F., Ryan, A.M., Carver-Moore, K. and Rosenthal, A (1996). Renal and neuronal abnormalities in mice lacking GDNF. Nature 382: 76-79.

Morgan, C.A., Parajuli, B., Buchman, C.D., Dria, K. and Hurley, T.D. (2015). N,N-diethylaminobenzaldehyde (DEAB) as a substrate and mechanism-based inhibitor for human ALDH isoenzymes. Chem Biol Interact 234: 18-28.

Natarajan, D., Marcos-Gutierrez, C., Pachnis, V. et al. (2002). Requirement of signaling by receptor tyrosine kinase RET for the directed migration of enteric nervous system progenitor cells during mammalian embryogenesis. Development 129(22): 5151-60.

Niederreither, K., Vermont, J., Le Roux, I., Schuhbaur, B., Chambon, P. and Dolle, P. (2003). The regional pattern of retinoic acid synthesis by RALDH2 is essential for the development of posterior pharyngeal arches and the enteric nervous system. Development 130: 2525-34.

Obermayr, F., Hotta, R., Enomoto, H. and Young, H.M. (2012). Development and developmental disorders of the enteric nervous system. Nature Reviews Gastroenterology and Hepatology 10: 43-57.

Oehlers, S.H., Cronan, M.R., Scott, N.R., Thomas, M.I., Okuda, K.S., Walton, E.M., Beerman, R.W., Crosier, P.S., Tobin, D.M. (2014) Interception of host angiogenic signalling limits mycobacterial growth. Nature. 517(7536):612-5.

Olden, T., T. Akhtar, S. A. Beckman and K. N. Wallace (2008). Differentiation of the zebrafish enteric nervous system and intestinal smooth muscle. Genesis 46(9): 484-498.

Olsson, C., A. Holmberg and S. Holmgren (2008). Development of enteric and vagal innervation of the zebrafish (Danio rerio) gut. J Comp Neurol 508(5): 756-770.
Pachnis, V., Durbec, P., Taraviras, S., Grigoriou, M. and Natarajan, D. (1998). III. Role of the RET signal transduction pathway in development of the mammalian enteric nervous system. Am J Physiol 275(2 pt 1): G183-6.
Peters-Van Der Sanden, M.J., Kirby, M.L., Gittenberger-De Groot, A., Tibboel, D., Mulder, M.P. and Meijers, C. (1993). Ablation of various regions within avian vagal neural crest has differential effects on ganglion formation in the fore-, mid- and hindgut. Dev Dynamics 196:183-194.
Pichel, J.G., Shen, L., Sheng, H.Z., Granholm, A.C., Drago, J., Grinberg, A., Lee, E.J., Huang, S.P., Saarma, M., Hoffer, B.J., Sariola, H. and Westphal, H. (1996). Defects in enteric innervation and kidney development in mice lacking GDNF. Nature 382:73-76.
Qin, P., Cimildoro, R., Kochhar, D.M., Soprano, K.J. and Soprano, D.R. PBX, MEIS, and IGF-I are potential mediators of retinoic acid-induced proximodistal limb reduction defects. Teratology 66(5):224-34.
Rauch, G. J., Lyons, D.A., Middendorf, I., Friedlander, B., Arana, N., Reyes, T., and Talbot, W.S (2003). Submission and Curation of Gene Expression Data. zfin.org
Reichenbach, B., J. M. Delalande, E. Kolmogorova, A. Prier, T. Nguyen, C. M. Smith, J. Holzschuh and I. T. Shepherd (2008). Endoderm-derived Sonic hedgehog and mesoderm Hand2 expression are required for enteric nervous system development in zebrafish. Dev Biol 318(1): 52-64.
Robertson, K. and Mason, I. (1995). Expression of ret in the chicken embryo suggests roles in regionalisation of the vagal neural tube and somites and in development of multiple neural crest and placodal lineages. Mech of Dev 53:329-344.
Sakaguchi, T., Kikuchi, Y., Kuroiwa, A., Takeda, H., and Stainier, D.Y. (2006) The yolk syncytial layer regulates myocardial migration by influencing extracellular matrix assembly in zebrafish. Development 133(20):4063-4072.
Saint-Jeannet, J.P. (2006). Advances in Experimental Medicine and Biology: Neural Crest Induction and Differentiation. Landes Bioscience and Springer Science+Business Media, New York, New York.
Sanchez, M.P., Silos-Santiago, I., Frisen, J., He, B., Lira, S.A. and Barbacid, M. (1996). Renal agenesis and the absence of enteric neurons in mice lacking GDNF. Nature 382: 70-73.
Sasselli, V., Pachnis, V. and Burns, A.J. (2012). The enteric nervous system. Developmental Biology 366 (1): 64-73.
Sato, Y. and Heuckeroth, R.O. (2008). Retinoic Acid regulated murine enteric nervous system precursor proliferation, enhances neuronal precursor differentiation, and reduces neurite growth in vitro. Developmental Biology 320 (1): 185-98.
Schilling, T.F., Nie, Q. and Lander, A.D. (2012). Dynamics and precision in retinoic acid morphogen gradients. Curr Opin Genet Dev 22 (6): 562-569.
Shepherd, I. T., C. E. Beattie and D. W. Raible (2001). Functional analysis of zebrafish GDNF. Dev Biol 231(2): 420-435.
Schuchardt, A., D'Agati, V., Larsson-Blomberg, L., Costanini, F. and Pachnis, V. (1994). Defects in kidney and enteric nervous system of mice lacking the tyrosine kinase receptor Ret. Nature 367: 380-383.
Seiler, C., Abrams, J. and Pack, M. (2010). Characterization of zebrafish intestinal smooth muscle development using a novel sm22α-β promoter. Dev Dynamics 239:2806-2812.

947 Shepherd, I. T., J. Pietsch, S. Elworthy, R. N. Kelsh and D. W. Raible (2004). Roles for
948 GFRalpha1 receptors in zebrafish enteric nervous system development. Development
949 131(1): 241-249.
950 Simkin, J.E., Zhang, D., Rollo, B.N., Newgreen, D.F., 2013. Retinoic acid upregulates ret
951 and induces chain migration and population expansion in vagal neural crest cells to
952 colonise the embryonic gut. PLoS One 8, e64077.
953 Southard-Smith, E.M., Kos, L. and Pavan, W.J. (1998). Sox10 mutation disrupts neural
954 crest development in Dom Hirschsprung mouse model. Nat Genetics 18(1): 60-4.
955 Taraviras, S. and Pachnis, V. (1999). Development of the mammalian enteric nervous
956 system. Curr Opin Genet Dev 9(3): 321-27.
957 Taylor, C.R., Montagne, W.A., Eisen, J.S. and Ganz, J. (2016). Molecular fingerprinting
958 delineates progenitor populations in the developing zebrafish enteric nervous system.
959 Developmental Dynamics 245(11): 1081-1096.
960 Tucker, G.C., Ciment, G. and Thiery, J.P. (1986). Pathways of avian neural crest cell
961 migration in the developing gut. Dev Biol 116:439-450.
962 Uesaka, T., Young, H.M., Pachnis, V. and Enomoto, H. (2016). Development of intrinsic
963 and extrinsic innervation of the gut. Developmental Biology 417(2): 158-67.
964 Uribe, R.A. and Bronner, M.E. (2015). Meis3 is required for neural crest invasion of the
965 gut during zebrafish enteric nervous system development. Molecular Biology of the Cell.
966 26(21):3728-40.
967 Uyttebroek, L., Shepherd, I.T., Harrison, F., Hubens, G., Blust, R., Timmermans, J.P. and
968 Van Nassauw, L. (2010). Neurochemical coding of enteric neurons in adult and
969 embryonic zebrafish (Danio rerio). The Journal of Comparative Neurology 518: 4419-38.
970 van der Velden, Y.U., Wang, L., van Lohuizen, M., Haramis, A.P., 2012. The Polycomb
971 group protein Ring1b is essential for pectoral fin development. Development 139, 2210-
972 2220.
973 Villefranc JA, Nicoli S, Bentley K, Jeltsch M, Zarkada G, Moore JC, Gerhardt H, Alitalo K,
974 Lawson ND. A truncation allele in vascular endothelial growth factor c reveals distinct
975 modes of signaling during lymphatic and vascular development Development. 2013
976 Apr;140(7):1497-506
977 Vohra, B.P., Fu, M. and Heuckeroth, R.O. (2007). Protein kinase Czeta and glycogen
978 synthase kinase-3beta control neuronal polarity in developing rodent enteric neurons,
979 whereas SMAD specific E3 ubiquitin protein ligase1 promotes neurite growth but does
980 not influence polarity. Journal of Neuroscience 27: 9458-68.
981 Wakamatsu, N., Yamada, Y., Ono, T., Nomura, N., Taniguchi, H., Kitoh, H., Mutoh, N.,
982 Yamanaka, T., Mushiake, K., Kato, K., Sonta, S. and Nagaya, M. (2001). Mutations in
983 SIP1, encoding Smad-Interacting protein-1, cause of a form of Hirschsprung disease. Nat
984 Genet 27(4): 369-70.
985 Waxman, J.S., Keegan, B.R., Roberts, R.W., Poss, K.D., Yelon, D., 2008. Hoxb5b acts
986 downstream of retinoic acid signaling in the forelimb field to restrict heart field potential in
987 zebrafish. Dev Cell 15, 923-934.
988 Worley, D.S., Pisano, J.M., Choi, E.D., Walus, L., Hession, C.A., Cate, R.L., Sanicola, M.,
989 and Birren, S.J. (2000). Developmental regulation of GDNF response and receptor
990 expression in the enteric nervous system. Development 127(20): 4383-93.
991 Yin, C., Kikuchi, K., Hochgreb, T., Poss, K.D., and Stainier, D.Y. (2010) Hand2 Regulates
992 Extracellular Matrix Remodeling Essential for Gut-Looping Morphogenesis in Zebrafish.
993 Developmental Cell. 18(6):973-984.

994 Young, H.M., Bergner, A. J., Simpson, M.K., Mckeown, S.J., Hao, M.M., Anderson C.R.
995 and Enomoto, H. (2014). Colonizing while migrating: how do individual enteric neural
996 crest cell behave? BMC Biology 12:23.
997 Zimmer, J. and Puri, P. (2015). Knockout mouse models of Hirschsprung's Disease.
998 Pediatr Surg Int (2015) 31: 787-794.
999

1000 **Figure 1. RA pathway components are expressed along the gut during ENS**

1001 **development**.

1002 (A) Cartoon illustration of a 1-dpf zebrafish embryo depicted laterally to reveal the

1003 location of the foregut, midgut and hindgut. ot-otic, d-dorsal, v-ventral, a-anterior, p-

1004 posterior

1005 (B) Whole-mount *in situ* hybridization against *aldh1a2* at 48 hpf reveals its localization

1006 along all levels of the gut tube.

1007 (C) Whole-mount *in situ* hybridization against *rbp5* at 48 hpf reveals its localization along

1008 all levels of the gut tube.

1009 (D) Whole-mount *in situ* hybridization against *crabp2a* at 48 hpf reveals its localization

1010 along the foregut.

1011 (E-E'') Cryosection through the level of the foregut depicts Aldh1a2 protein localization

1012 (red) in the gut mesenchyme (m), but not in the gut endoderm (e), marked by *sox17*:GFP.

1013 s-somite, yk-yolk

1014 (F-F'') Cryosection through the level of the foregut depicts Aldh1a2 protein localization

1015 (red) in the gut mesenchyme (m) and within neural crest cells migrating in the gut

1016 mesenchyme (arrows), marked by *sox10*:GFP. s-somite, yk-yolk.

1017 Scale bars: 50 μM

1018

1019 **Figure 2. RA treatment during enteric neural crest migration stages enhances**

1020 **enteric neuron numbers**

(A-B) A dorsal view following whole-mount *in situ* hybridization at 48 hpf for *crestin* in control (A) and RA-treated larvae (B) reveals neural crest localization along the embryo. RA-treated embryos display an expansion of neural crest, arrows (B), when compared to control (A). vg-vagal

(C-D) Cryosections through the foregut of larvae at 52 hpf following in situ hybridization for *crestin* in (C) control and (D) RA-treated larvae shows an expanded distribution of *crestin*$^{+}$ neural crest near the vicinity of the gut (arrows), when compared with control larvae. NT- neural tube

(E-F) Transverse sections depicting the localization of *sox10*:GFP^{+} neural crest in (E) control and (F) RA-treated larvae shows an expansion of neural crest near the vicinity of the gut (arrows), when compared with control larvae. Scale bars, 50 μM

(G) Bar graph to represent the average number of Hu^{+} and 5HT^{+} neurons along the gut in control and RA-treated larvae at 96 hpf. Error bars indicate +/- S.E.M. , *n*=6 embryos for each condition.

(H-I) Lateral views of the gut at 96 hpf following whole-mount antibody staining to detect Hu^{+}/5HT^{+} enteric neurons in (H-H'') control and (I-I'') RA-treated larvae.

(J) Zoomed in view of control larval fish depicted in H.

(K) Zoomed in view of RA-treated larval fish depicted in I.

Scale bars, 50 μM.

Figure 3. Temporal loss of RA stalls migration of enteric neural crest within the foregut without affecting enteric neural crest cell numbers

(A-B) Whole-mount *in situ* hybridization against *crestin* in (A) control and (B) DEAB treated larvae at 52 hpf.

(C-D) Whole-mount *in situ* hybridization against *crestin* in control and DEAB treated larvae at 72 hpf reveals that enteric neural crest are delayed along the foregut, when compared with controls. Arrows and yellow asterisk marks caudal end of enteric neural crest migratory front along the gut. yk-yolk

(E-F) Live images of *-8.3phox2bb*:Kaede (E) control and (F) DEAB treated larvae at 72 hpf reveals that enteric progenitors are delayed in migration along the foregut, when compared with control cells along the hindgut. yk-yolk

(G-H) Live confocal projection images of *hand2*:GFP in (G) control and (H) DEAB treated larvae at 52 hpf reveals the presence of gut mesenchyme laterally along the gut.

(I-J) Transverse cryosections show that *sox10*:GFP^{+} cells located near the foregut in (I) control and (J) DEAB treated larvae. When compared with control sections, DEAB treated larvae exhibit increased numbers of neural crest in the mesenchyme surrounding the gut (yellow arrows), while number of neural crest in direct gut contact (white arrows) are not affected. s-somite, yk-yolk

(K) Bar graph depicting the average number of *sox10*:GFP^{+} neural crest with direct gut contact or in the surrounding ventral mesenchyme near the gut in control and DEAB treated larvae. *n*=9 embryos for each condition. Error bars indicate +/- S.E.M. *, $p < .05$ with Student's *t*-test.

(L) Bright field images of a control (top) and DEAB treated (bottom) larval fish at 48 hpf to reveal the distribution of melanophores.

Scale bars in panels E-H, 100 μM; scale bar in panel I-J, 30 μM.

Figure 4. Temporal inhibition of RA results in stalled migration of enteric neural crest chains and loss of chain formation along the foregut

(A) Cartoon schematic of a zebrafish larval fish to illustrate the timing and location of live imaging experiments in panels B-C. Enteric neural crest migratory front cells along the leading edge were imaged in control and experimental conditions.

(B-B',C-C') Cropped time lapse stills over the course of 3 hours showing the enteric neural crest chain front along the foregut-midgut of a *sox10*:GFP^{+} control larval fish (B-B') and the foregut a DEAB treated (C-C') larval fish. The DEAB treated enteric neural crest chain exhibits delayed migration along the foregut and solitary cells detached from the chain (arrows), while the control enteric neural crest chain front was observed migrating along the midgut collectively.

(D-E) Cell tracks of control (D) and DEAB treated (E) enteric neural crest show that DEAB treated enteric neural crest cells fail to progress caudally along the gut, when compared with control.

(F) Whole mount immunochemistry against RFP reveals that at 72 hpf, control enteric neural crest chains are maintained along the gut, while DEAB treated enteric neural crest have dissociated along the foregut.

(G) Cartoon schematic summarizing the neural crest chain migration phenotype observed following loss of RA along the gut. Red cells depict neural crest migrating in chains along the gut tube in control (top) and in DEAB treated fish (bottom). DEAB treated neural crest chains never make it past the foregut, where they become ectopically localized in the vicinity surrounding the gut.

Scale bar in B,C,D and E: 40 μM; scale bar in F: 50 μM.

Figure 5. Temporal loss of RA causes total intestinal aganglionosis

(A-B) Lateral view of the foregut of a control (A) and DEAB treated larval fish (B) following double immunochemistry against Hu (red) and 5HT (green) shows that control fish successfully differentiate enteric neurons, while DEAB treated fish lack almost all neurons. A small cluster of ~3 neurons was detected in the anterior foregut of the DEAB treated larval fish (arrow in B).

(C-D) Lateral view of the foregut of a control (C) and DEAB treated larval fish (D) following immunochemistry against Acetylated Tubulin shows that control fish contain differentiated enteric neurons, along with axons (arrows), while DEAB treated larval fish do not.

Scale bar in A and C: 30 μM. Anterior to the left.

Figure 6. RA depletion causes accumulation of enteric progenitors in the ventral mesenchyme near the foregut and their apoptosis

(A-A''-B-B'') At 52 hpf, transverse sections through the foregut of control (A-A'') and DEAB treated larvae (B-B'') reveal the location of *-8.3phox2bbb*:Kaede^{+}/Hu^{+} enteric progenitors (arrows),

(C-D) Bar graphs depict the average number of Kaede^{+} enteric progenitors (C) and Hu^{+} enteric neurons (D) in control and DEAB treated larval foregut sections. *n*=5 embryos for each condition. Error bars indicate +/- S.E.M. *, $p < .05$ with Student's *t*-test.

(E-E''-F-F'') Whole mount double immunochemistry against activated-Caspase3 (red) and GFP (green) in *sox10*:GFP control (E-E'") and DEAB treated (F-F'') larval fish. GFP^{+}/Caspase3^{+} cells are present along the foregut of DEAB treated fish, however not detected in control embryos.

(G-G'', H-H'') At 70 hpf, transverse sections through the foregut of control (G-G'') and DEAB treated larvae (H-H'') show the location of *sox10*:GFP^{+} and Caspase3^{+} cells (red), which reveals neural crest cells that are Caspase3^{+} surrounding the gut in DEAB treated fish, when compared to controls.

Scale bar in A, B, G-H: 20 μM; scale bar in E,F: 60 μM

Figure 7. RA modulates the spatial expression of *meis3* in the vagal and foregut tissue domains

(A-B) Following DEAB treatment from 24-52 hpf (B), the expression area of *meis3* in the vagal (vg) region (yellow arrow) and foregut tissue (white arrow) is diminished when compared with control larvae (A).

(C-D) Following heat shock induction, dnRaraa-GFP^{+} (D) larval fish exhibit a reduced expression domain of *meis3* along the foregut (arrowhead) and vagal region, when compared to heat shock controls.

(E-F) Following RA incubation from 24-48 hpf (F), the hindbrain expression of *meis3* was rostrally expanded (brackets), as well as the foregut (arrow), when compared with control larvae (E).

Figure 8. Ectopic expression of *meis3* and/or *ret* is sufficient to partially rescue gut colonization in embryos temporally lacking RA

(A-H) Maximum intensity confocal projection images show Hu^{+}/*-8.3phox2bb*:Kaede^{+} enteric neurons along the gut of (A) control larvae, (B) larvae expressing 40pg of *meis3*, (C) larvae expressing 50pg of *ret*, (D) larvae expressing 40pg *meis3* and 50 pg *ret*; (E) DEAB treated larvae, (F) DEAB treated larvae expressing 40pg *meis3*, (G)

DEAB treated larvae expressing 50 pg *ret*, (H) DEAB treated larvae expressing 40pg *meis3* and 50pg *ret*.

(E) Bar graphs depicting the percentage of larvae exhibiting normal colonization (neurons along whole length of gut), partial colonization (neurons present to the midgut) and no colonization (no neurons along the gut).

(J) Bar graphs showing the average number of neurons for the rescue conditions shown in A-H. Error bars indicate S.E.M. **, $p < .01$ with Student's *t*-test.

Scale bar in A-D: 60 μM.

Figure 9. Ectopic expression of *meis3* in the neural crest partially rescues gut colonization following RA inhibition

(A) Cartoon schematic summarizing injection and treatment experiments.

(B-C) Live images of *phox2bb*:Kaede/mCherry^{+} 24 hpf embryos injected with (B) *pDest-sox10:turq-P2A-mcherry-pA2*, or (C) *pDest-sox10:meis3-P2A-mcherry-pA2*. Lateral views, ot-otic.

(D-I) Maximum intensity confocal projections following immunochemistry against mCherry (red) and Hu (cyan) at 75 hpf in larvae expressing (D, F, H) *pDest-sox10:turq-P2A-mcherry-pA2*, or (E, G, I) *pDest-sox10:meis3-P2A-mcherry-pA2*, following treatment with DMSO or DEAB, respectively.

(H-I) Zoomed in view of the insets from F and G, respectively.

Scale bars: 60 μM

Figure 10. Stage-specific disruption of RA during neural crest entry and migration along the foregut, but not thereafter, leads to colonization defects

(A-D) Maximum intensity confocal projections reveal Hu^+ neurons in lateral views of the gut at 73 hpf in (A) Control larvae (DMSO treated), and larvae treated with DEAB from (B) 28-36 hpf, (C) 36-48 hpf, and (D) 48-73 hpf. Scale bar: 70 μM

(E) Bar graphs depicting the percentage of larvae exhibiting normal colonization (neurons along whole length of gut), partial colonization (neurons present to the midgut) and no colonization (no neurons along the gut).

(F) Cartoon illustration of the role of RA and Meis3 during enteric colonization of the gut. RA (cyan) is synthesized along the foregut mesenchyme (beige) concomitant with enteric neural crest (green) entry into the gut from the vagal neural crest domains. Meis3, functionally downstream of RA in the neural crest, and/or RET regulate caudal colonization of the gut during enteric nervous system development. The action of RA affects enteric colonization primarily during early foregut migration phases (28-48 hpf).

Movie 1: Neural crest migration along the control zebrafish larval gut.

Lateral view of *sox10*:$mRFP^+$ neural crest chains migrate caudally from the foregut through the midgut over the course of 9 hours. Neural crest chains successfully make their way from foregut to midgut in a smooth, collective chain.

Movie 2: Neural crest migration along the DEAB treated zebrafish larval gut.

Lateral view of *sox10*:mRFP+ neural crest chain migrate caudally down the foregut, however the enteric neural crest chain fails to progress into the midgut and over the course of 3 hours dissociates along the foregut, with individuals neural crest cells becoming ectopically localized away from the gut tube.

Movie 3: 3D animation depicting enteric neurons along the control zebrafish larval gut.

Rotation movie showing a lateral view of the 4dpf control larval fish foregut stained for Hu (red) and 5HT (green) positive neurons shown in Figure 5A.

Movie 4: 3D animation depicting enteric neurons along the DEAB treated zebrafish larval gut.

Rotation movie showing a lateral view of the 4dpf DEAB treated larval fish foregut stained for Hu (red) and 5HT (green) positive neurons shown in Figure 5B.

Movie 5: 3D animation depicting a control larval foregut following anti-Caspase immunostaining.

Rotation movie showing a lateral view of the 70 hpf control *sox10*:GFP^{+} larval fish foregut shown in Figure 6E stained for GFP (green) and activated Caspase3 (red).

Movie 6: 3D animation depicting a DEAB treated larval foregut following anti-Caspase immunostaining.

Rotation movie showing a lateral view of the 70 hpf DEAB treated *sox10*:GFP^{+} larval fish foregut shown in Figure 6E stained for GFP (green) and activated Caspase3 (red).

Figure S1. Heat shock attenuation of RA signaling function leads to delayed colonization of the gut by enteric neural crest cells.

(A-B) *crestin* whole-mount *in situ* hybridization in control heat shock (GFP^{-}) larvae (A) and heat shock dnRaraa-GFP^{+} larvae (B) at 48 hpf, arrowhead points to anterior foregut

region. Dorsal views reveal that neural crest cell entry along the foregut is delayed (arrows) in dnRaraa-GFP^{+} larvae (B'), when compared with control larvae (A'). vg-vagal, fb-fin bud

(C) Cartoon schematic to depict genotype and time course of heat shock attenuation experiments shown in panels D-G.

(D-G) Live confocal images showing *sox10*:mRFP$^{-/+}$; *hsp70*:dnRaraa-GFP$^{-/+}$ larvae at 52 hpf to reveal enteric neural crest chain localization along the gut. Lateral views show that enteric neural crest reside within the foregut following heat shock induction of dnRaraa-GFP, while control heat shock enteric neural crest are located within the midgut at the same time, asterisks denote caudal end of the migratory chain.

Scale bar in D and F, 100 microns; in E and G, 50 microns.

Figure S2. Ectopic expression of 25 pg of *meis3* is sufficient to partially rescue gut colonization in embryos temporally lacking RA

(A-D'') Whole mount double immunochemistry shows Hu^{+}/*-8.3phox2bb*:Kaede^{+} enteric neurons along the gut of (A-A'') control, (B-B'') DEAB treated larvae, (C-C'') larvae injected with 25 pg *meis3*, and larvae injected with 25 pg *meis3* and treated with DEAB (D-D''). While larvae treated with DEAB from 24-73 hpf exhibit a severe loss of enteric neurons (B-B''), embryos treated with DEAB also expressing 25 pg *meis3* exhibit a partial rescue of enteric neuron localization along the midgut (D-D'').

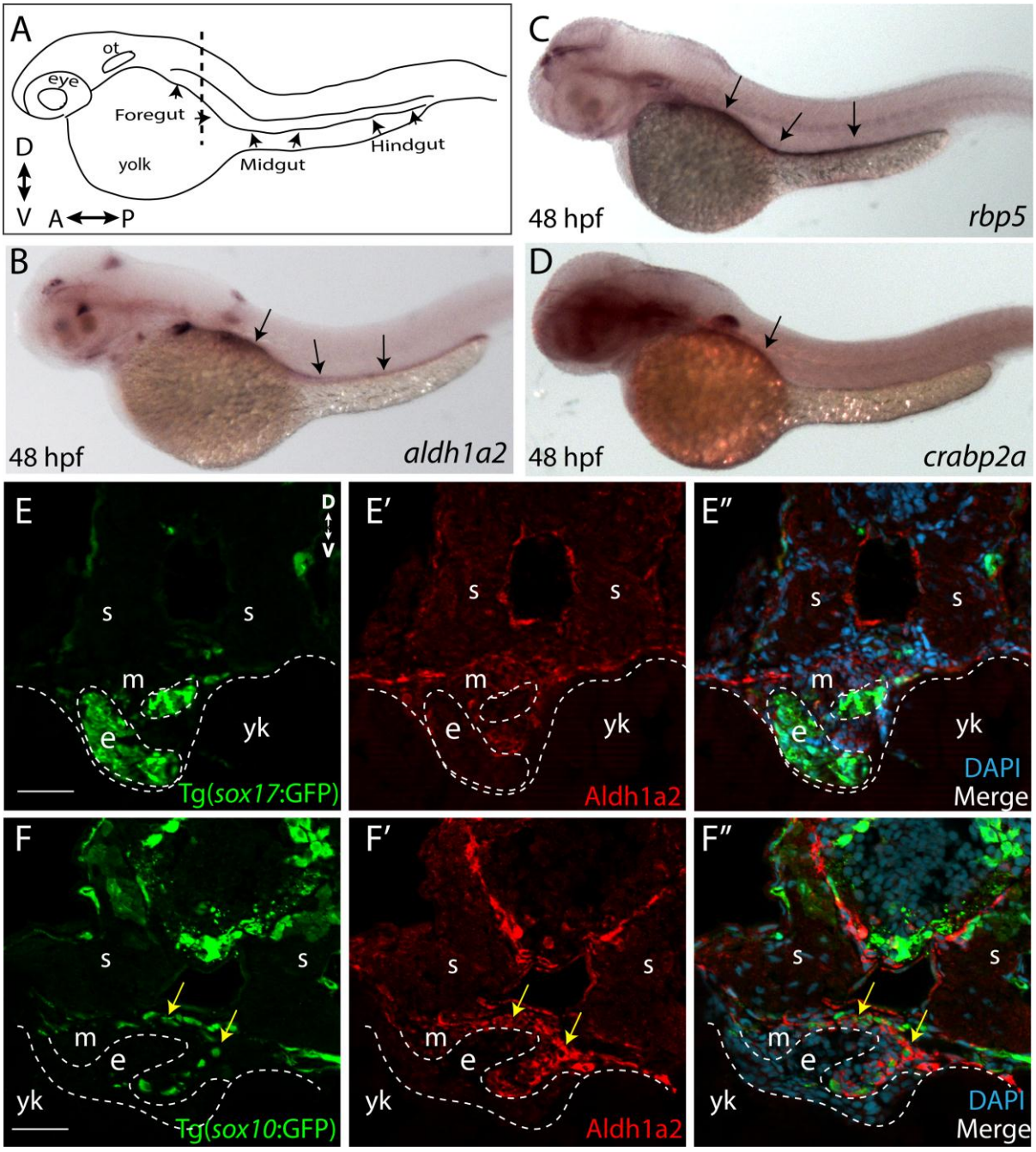
A
ot
eye
Foregut
Hindgut
D
yolk
Midgut
V A P
C
48 hpf
rbp5
B
48 hpf
aldh1a2
D
48 hpf
crabp2a
E
D
V
s
s
m
e
yk
Tg(sox17:GFP)
E′
s
s
m
e
yk
Aldh1a2
E″
s
s
m
e
yk
DAPI
Merge
F
s
s
m
e
yk
Tg(sox10:GFP)
F′
s
s
m
e
yk
Aldh1a2
F″
s
s
m
e
yk
DAPI
Merge

1232

1233

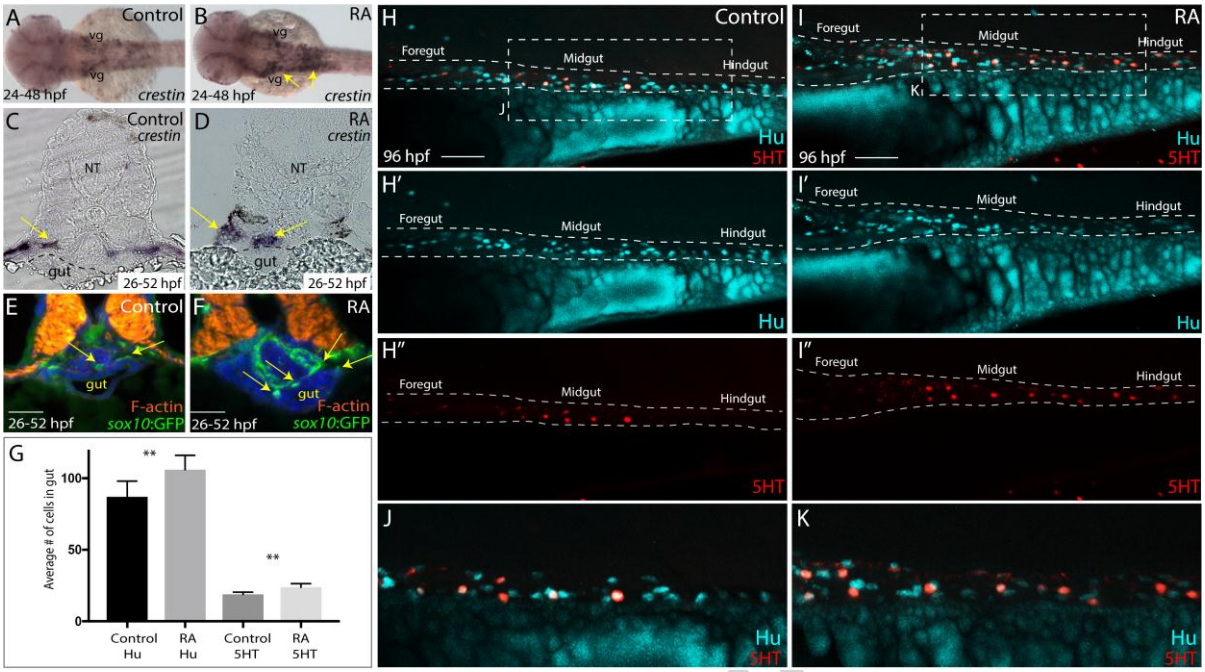

1234

1235

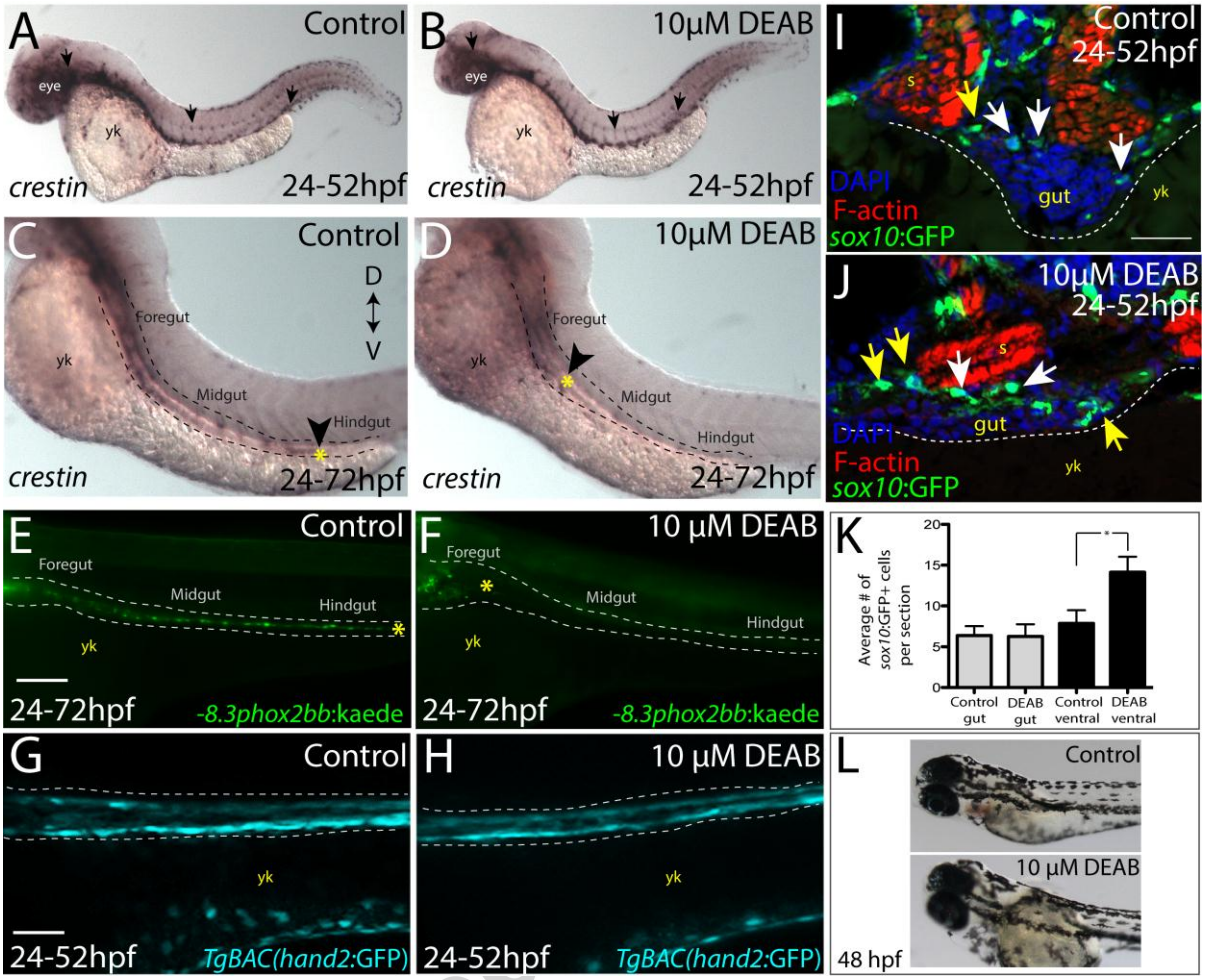

1236

1237

1238

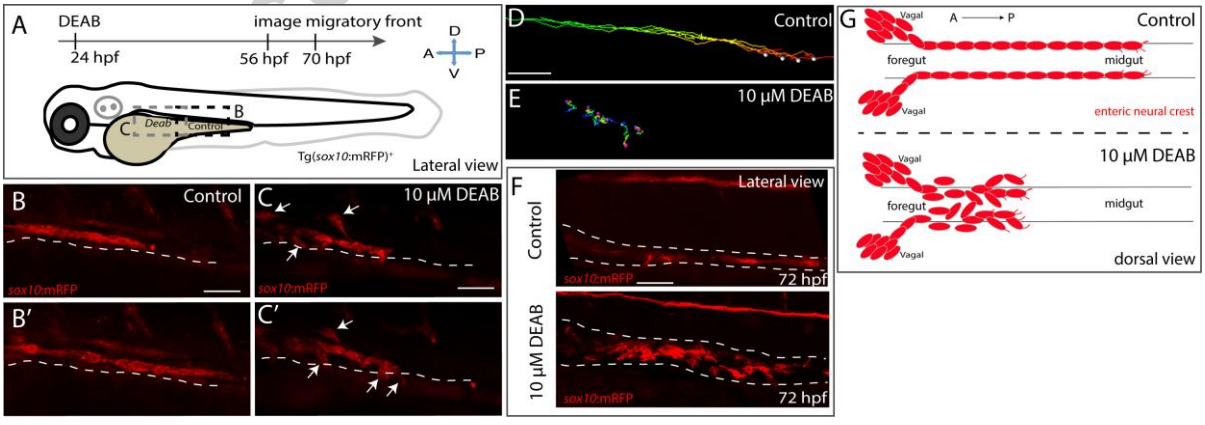

1239

1240

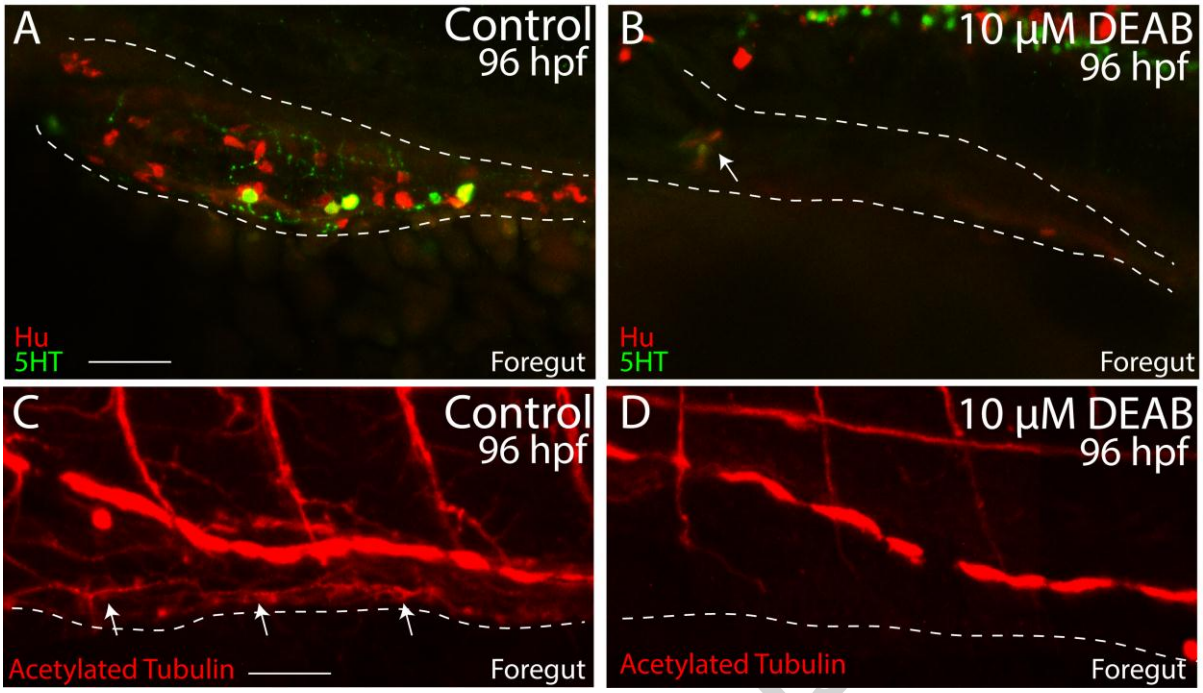

1241

1242

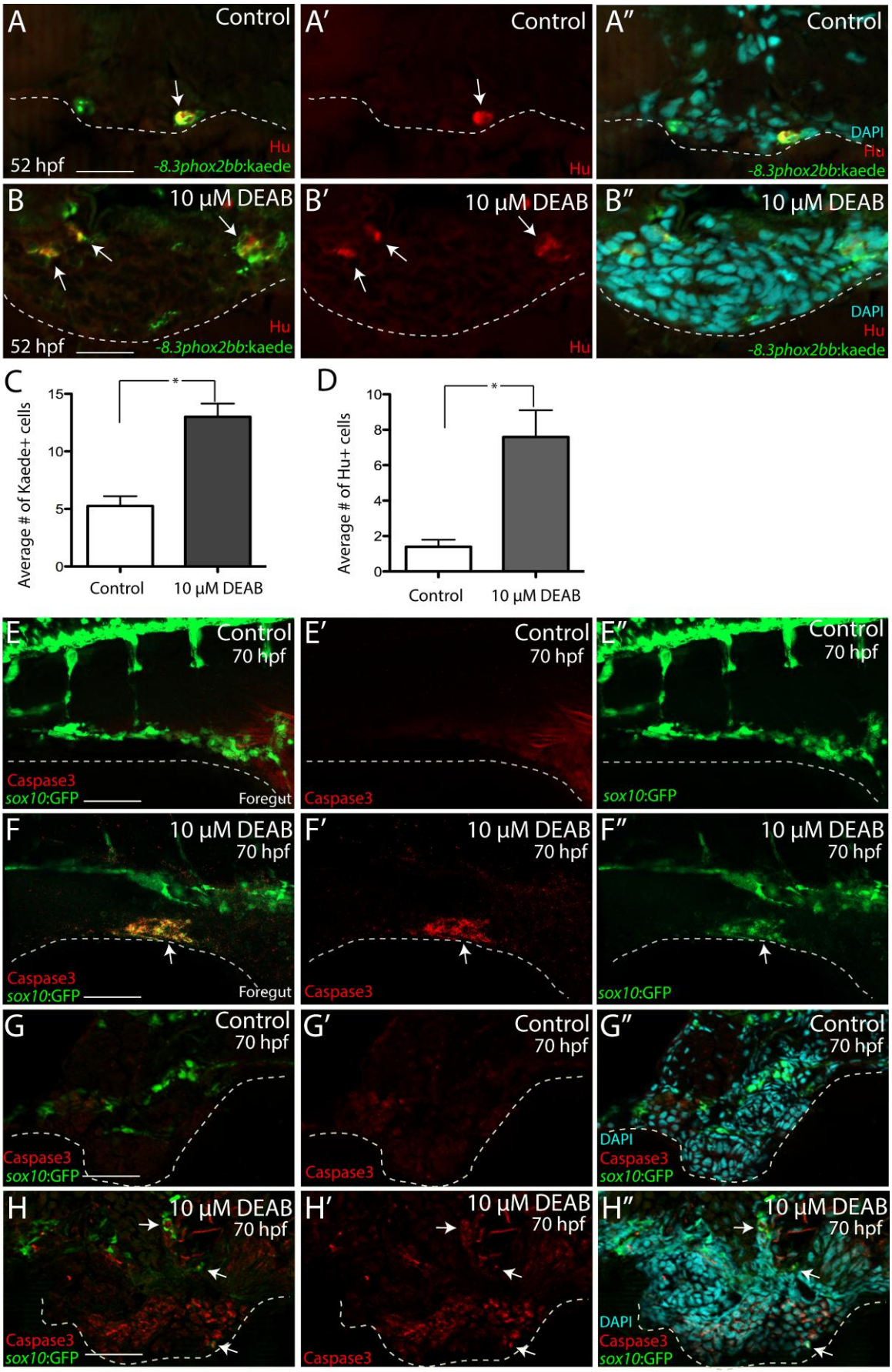
A
Control
Hu
52 hpf
-8.3phox2bb:kaede
A′
Control
Hu
A″
Control
DAPI
Hu
-8.3phox2bb:kaede
B
10 μM DEAB
Hu
52 hpf
-8.3phox2bb:kaede
B′
10 μM DEAB
Hu
B″
10 μM DEAB
DAPI
Hu
-8.3phox2bb:kaede
C
Average # of Kaede+ cells
15
10
5
0
*
Control
10 μM DEAB
D
Average # of Hu+ cells
10
8
6
4
2
0
*
Control
10 μM DEAB
E
Control
70 hpf
Caspase3
sox10:GFP
Foregut
E′
Control
70 hpf
Caspase3
E″
Control
70 hpf
sox10:GFP
F
10 μM DEAB
70 hpf
Caspase3
sox10:GFP
Foregut
F′
10 μM DEAB
70 hpf
Caspase3
F″
10 μM DEAB
70 hpf
sox10:GFP
G
Control
70 hpf
Caspase3
sox10:GFP
G′
Control
70 hpf
Caspase3
G″
Control
70 hpf
DAPI
Caspase3
sox10:GFP
H
10 μM DEAB
70 hpf
Caspase3
sox10:GFP
H′
10 μM DEAB
70 hpf
Caspase3
H″
10 μM DEAB
70 hpf
DAPI
Caspase3
sox10:GFP

1243

1244

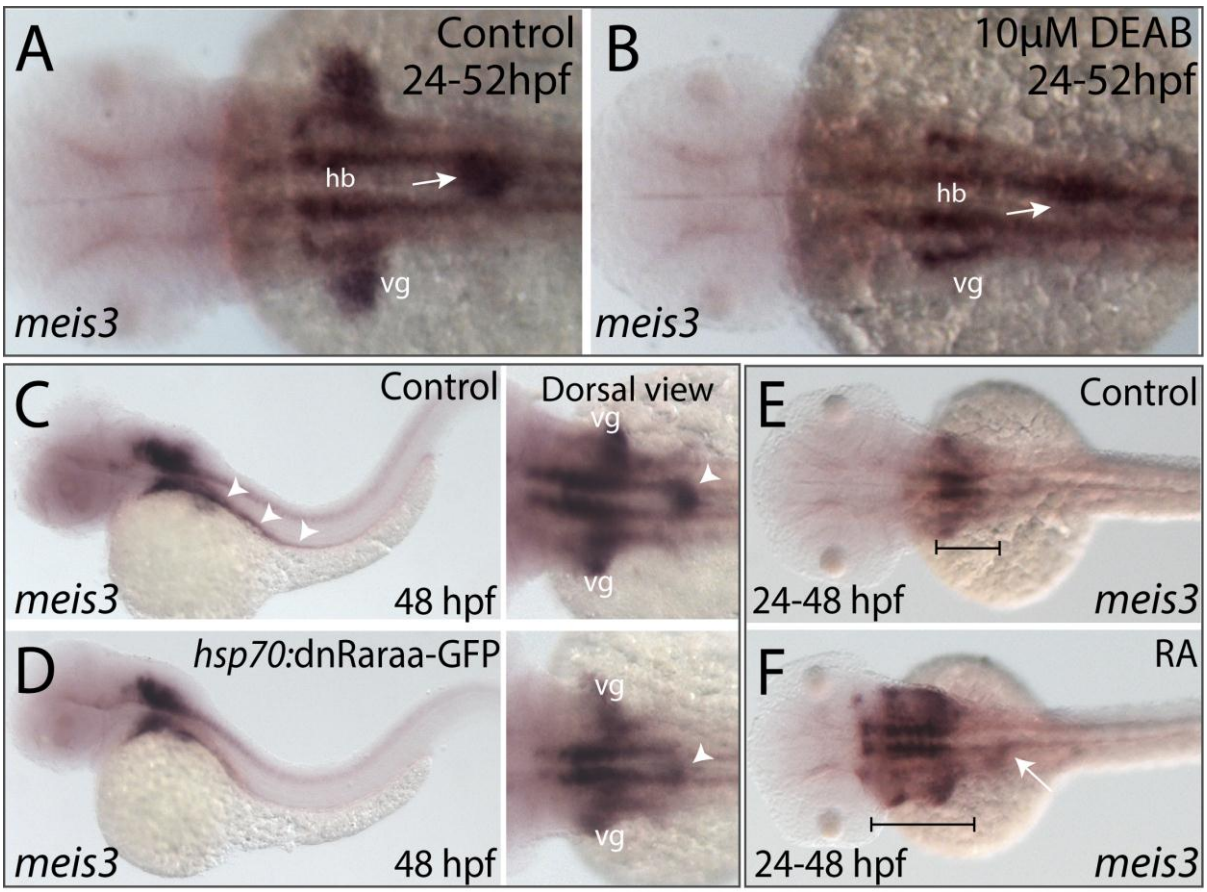

1245

1246

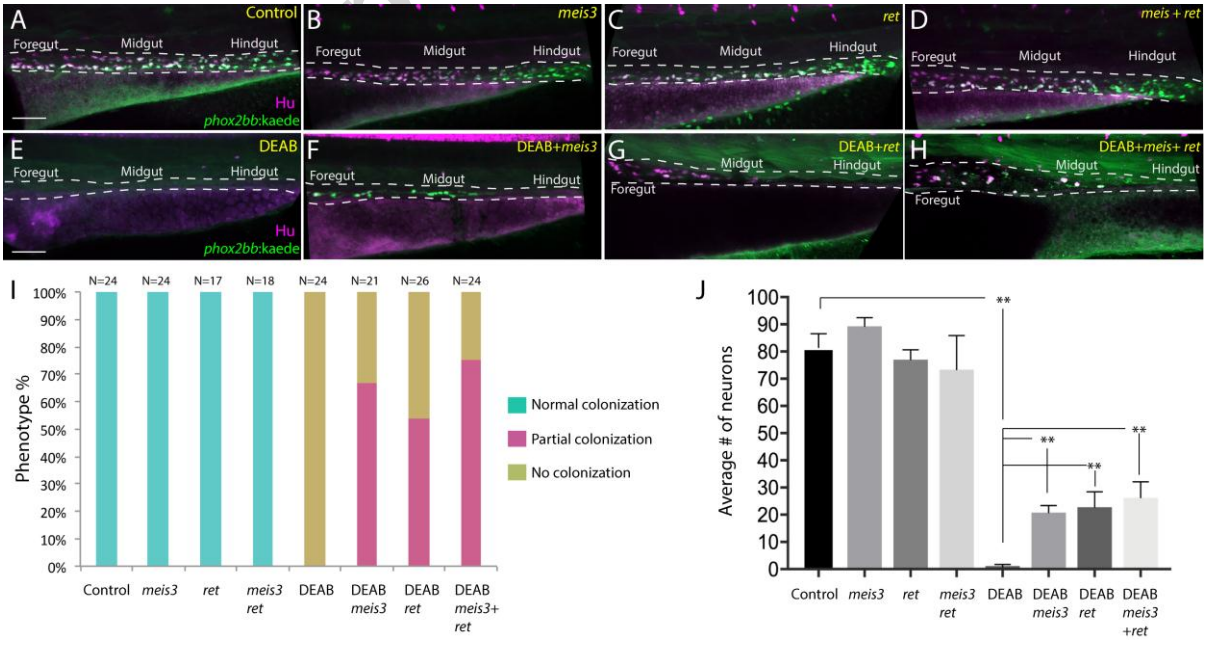

1247

1248

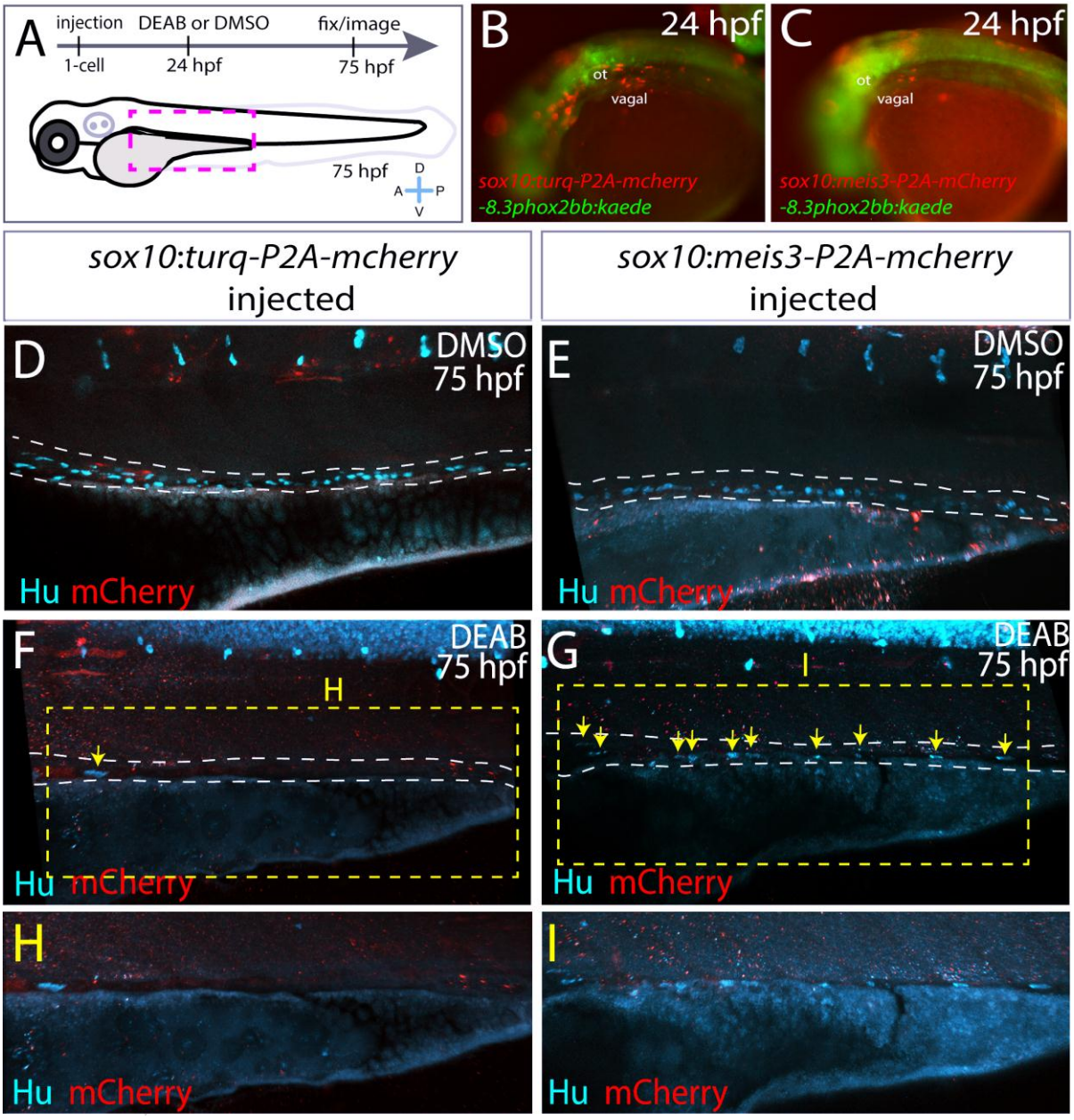

1249

1250

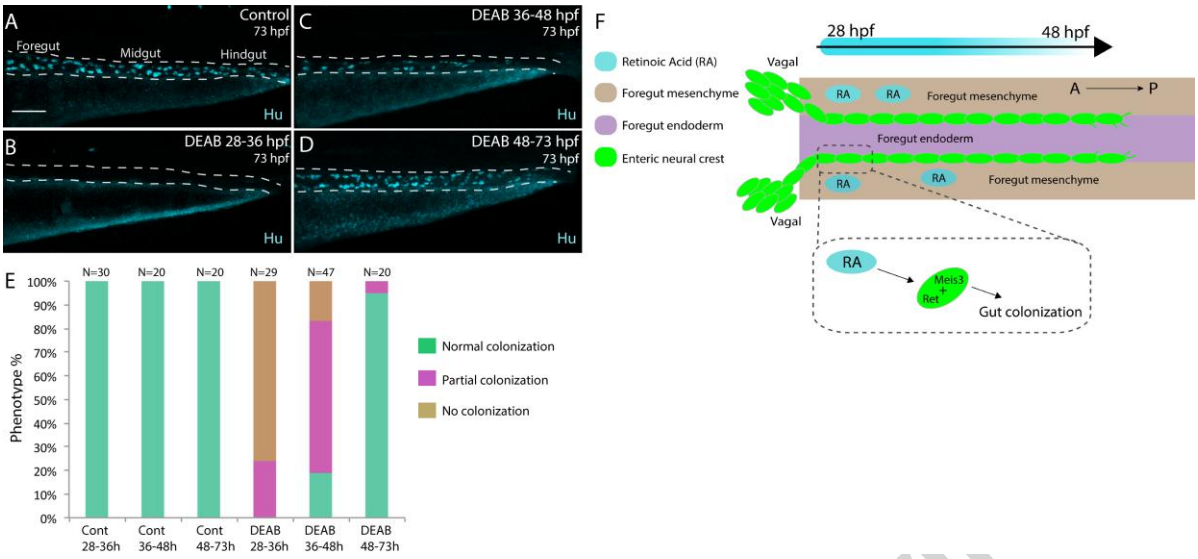

1251

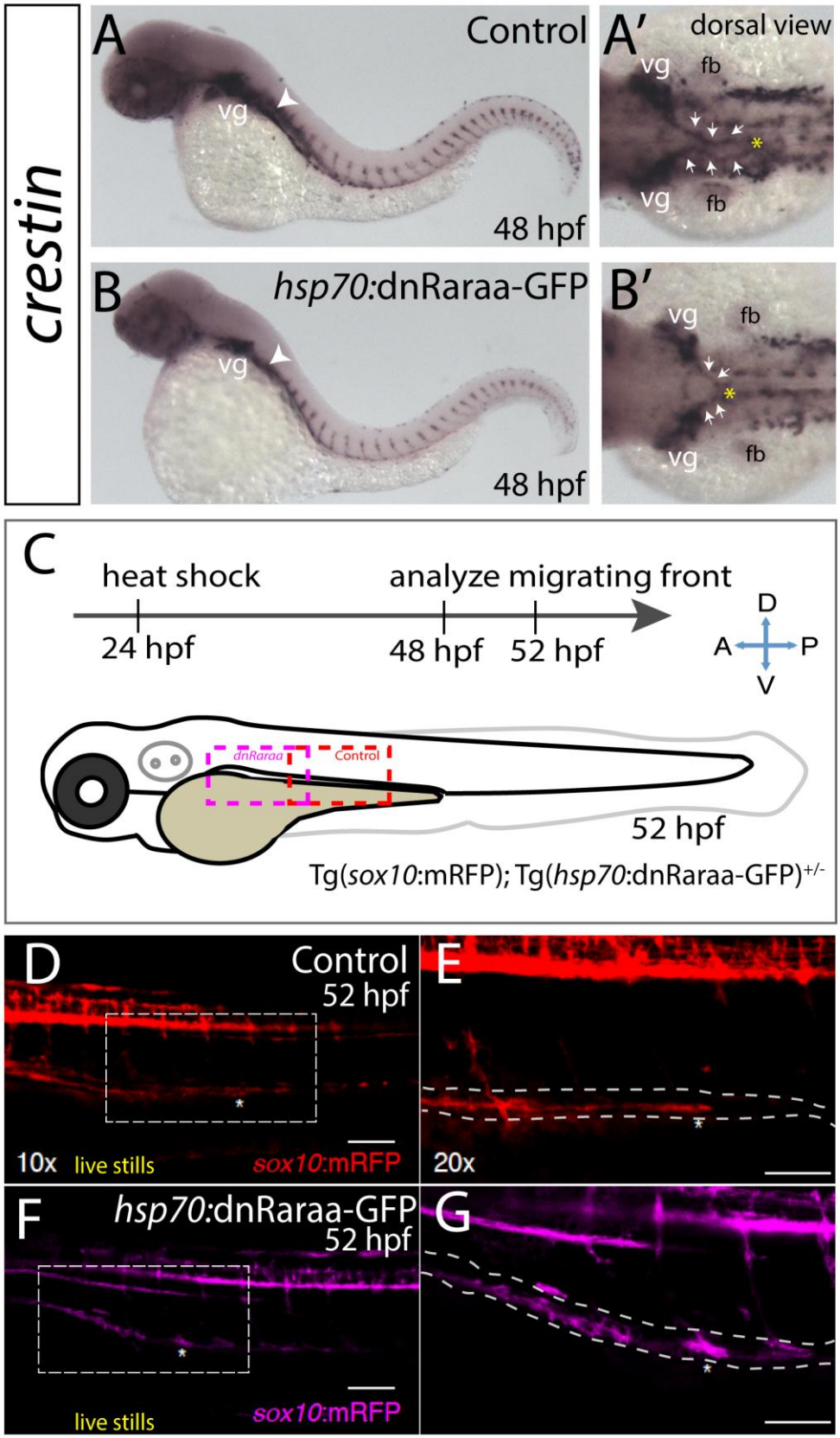
crestin
A
Control
vg
48 hpf
A′
dorsal view
vg
fb
vg
fb
B
hsp70:dnRaraa-GFP
vg
48 hpf
B′
vg
fb
vg
fb
C
heat shock
analyze migrating front
24 hpf
48 hpf
52 hpf
D
A
P
V
dnRaraa
Control
52 hpf
Tg(sox10:mRFP); Tg(hsp70:dnRaraa-GFP)+/-
D
Control
52 hpf
10x
live stills
sox10:mRFP
E
20x
F
hsp70:dnRaraa-GFP
52 hpf
live stills
sox10:mRFP
G

1252

1253

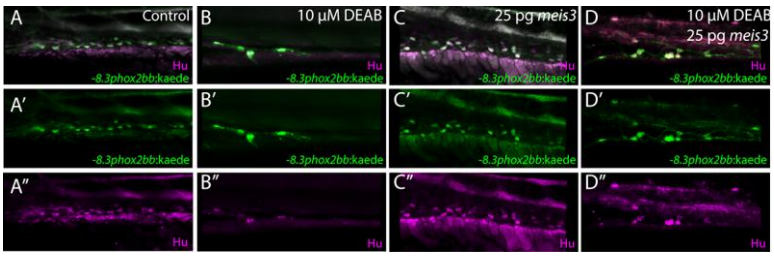

1254

1255

1256